Chemical Science

ROYAL SOCIETY OF CHEMISTRY

PERSPECTIVE

View Article Online
View Journal | View Issue

Cite this: *Chem. Sci.*, 2025, **16**, 7106

All publication charges for this article have been paid for by the Royal Society of Chemistry

Polymersome-based nanomotors: preparation, motion control, and biomedical applications

Siyu Song,†[b] Hao Han,†[a] Jianhong Wang,[c] Yubin Pu,[a] Jingxin Shao,[c] Jing Xie,*[d] Hailong Che,*[e] Jan C. M. van Hest*[c] and Shoupeng Cao*[a]

Polymersome-based nanomotors represent a cutting-edge development in nanomedicine, merging the unique vesicular properties of polymersomes with the active propulsion capabilities of synthetic nanomotors. As a vesicular structure enclosed by a bilayer membrane, polymersomes can encapsulate both hydrophilic and hydrophobic cargoes. In addition, their physical–chemical properties such as size, morphology, and surface chemistry are highly tunable, which makes them ideal for various biomedical applications. The integration of motility into polymersomes enables them to actively navigate biological environments and overcome physiological barriers, offering significant advantages over passive delivery platforms. Recent breakthroughs in fabrication techniques and motion control strategies, including chemically, enzymatically, and externally driven propulsion, have expanded their potential for drug delivery, biosensing, and therapeutic interventions. Despite these advancements, key challenges remain in optimizing propulsion efficiency, biocompatibility, and *in vivo* stability to translate these systems into clinical applications. In this perspective, we discuss recent advancements in the preparation and motion control strategies of polymersome-based nanomotors, as well as their biomedical-related applications. The molecular design, fabrication approaches, and nanomedicine-related utilities of polymersome-based nanomotors are highlighted, to envisage the future research directions and further development of these systems into effective, precise, and smart nanomedicines capable of addressing critical biomedical challenges.

Received 6th December 2024
Accepted 2nd April 2025

DOI: 10.1039/d4sc08283d

rsc.li/chemical-science

Introduction

Biological systems serve as abundant sources of inspiration for scientists seeking to design synthetic analogs with biomimetic properties to perform specific functions.[1–4] Such biomimicry is often achieved *via* molecular self-assembly to afford complex structures *via* adapting biological principles and mechanisms.[5–8] One prominent research area in this regard is the self-assembly of amphiphilic block copolymers (BCPs).[9,10] Innovations in controlled polymerization techniques—such as atom transfer radical polymerization (ATRP), reversible addition-fragmentation chain transfer (RAFT), and ring-opening polymerization (ROP)—have made it possible to precisely synthesize a wide variety of amphiphilic BCPs.[11–14] By fine-tuning the composition, molecular weight, polydispersity index, and topological features of BCPs, a diverse array of self-assembled structures can be created, including spherical micelles, cylindrical micelles, lamellae, bilayer vesicles, and inverse mesophases.[15–18] The physical and chemical properties of these BCP-based assemblies—such as size, morphology, stability, surface chemistry, flexibility, and responsiveness to environmental stimuli—can be readily adjusted to meet the demands of various technical and biomedical applications.

Polymeric vesicles, also known as polymersomes, contain a hollow interior surrounded by a bilayer membrane self-assembled from amphiphilic BCPs, resembling the structure of biological compartments.[19,20] They usually display a nanometer size rang (30–1000 nm) but can also be attained with micro-meter size (1–100 μm) comparable to living cells.[21–23] Polymersomes can not only encapsulate and protect a variety of hydrophilic cargoes (*e.g.*, enzymes, proteins, DNAs, and RNAs) in their lumen, but also load hydrophobic species (emissive agents, molecular drugs) in their membrane pocket.[24] This allows polymersomes to find numerous applications in various fields, including synthetic biology, material science, and

[a]*College of Polymer Science and Engineering, State Key Laboratory of Polymer Materials Engineering, Sichuan University, Chengdu 610065, PR China. E-mail: caoshoupeng@scu.edu.cn*

[b]*Life-Like Materials and Systems, Department of Chemistry, University of Mainz, Mainz, 55128, Germany*

[c]*Bio-Organic Chemistry, Institute of Complex Molecular Systems, Eindhoven University of Technology, Helix, P. O. Box 513, Eindhoven, 5600 MB, The Netherlands. E-mail: J.C.M.v.Hest@tue.nl*

[d]*Institute of Biomedical Engineering, West China School of Basic Medical Sciences & Forensic Medicine, Sichuan University, Chengdu 610041, China. E-mail: jingxie@scu.edu.cn*

[e]*Department of Chemical Engineering, School of Environmental and Chemical Engineering, Shanghai University, Shanghai 200444, China. E-mail: hche@shu.edu.cn*

† Siyu Song and Hao Han contribute to this work equally.

nanomedicine.[25–27] The chemical versatility of BCPs allows facile modulation of their chemical elements and tunable chain length, which can endow polymersomes with several key features such as environmental responsiveness and permeability control.[28,29] This is of particular importance for polymersomes to delivery and release of therapeutic agents at the desired site of action.[30–32] Surface chemical modification of polymersomes with ligands (such as folic acid, biotin, and RGDs) can further boost the delivery efficiency to targeted cells.[33,34]

However, traditional drug delivery systems often suffer from limited targeting efficiency, poor penetration in biological barriers, and passive diffusion-based transport, which limited delivery efficiency leading to a decrease in effective therapeutic concentration and undesired treatment efficacy. Nanomotors-based delivery strategies address these challenges by integrating active propulsion mechanisms, enabling autonomous movement and precise navigation toward target sites.[35–37] They display a capacity to convert various sources of energy into active motion, relying on chemical/enzymatic reactions or external stimuli (*e.g.*, light, magnetic fields, or ultrasound) to propel themselves.[38–43] These particulate systems, capable of active transportation, are promising entities that show significant advantages in a variety of complex tasks, including targeting, drug delivery, diagnostics, and overcoming biological barriers.[44–47] For example, enzyme-powered polymersome nanomotors can respond to specific biological triggers, enhancing drug release at diseased tissues, while magnetically or light-driven systems allow for remote control of movement, improving accumulation at target locations.[41,48–50] These capabilities significantly enhance drug bioavailability, reduce off-target effects, and improve therapeutic efficacy compared to conventional passive delivery platforms.

Self-propulsion of nanomotors is essentially realized by the design of an asymmetrical structure, which allows for the implementation of a directional net force on the particle.[51–53] This can be a result of the asymmetric design of the scaffold itself or the asymmetric distribution of active moieties on the motor.[54–56] Synthetic micro/nano motors are usually constructed with metals like platinum, gold, and silver, due to their inherent catalytic properties and facile functionalization.[57–60] Platinum, for example, has been commonly used in the fabrication of hydrogen peroxide-powered motors, where it acts as a catalyst to decompose H_2O_2 into oxygen and water, inducing propulsion.[61] Although metal-based nanomotors demonstrated effectiveness in self-propulsion, their inherent properties such as non-biocompatibility and non-biodegradability pose considerable challenges and accumulation could potentially even lead to toxicity in biological systems.[62] In this regard, there is a growing interest in using biocompatible, polymeric, or hybrid materials to overcome the limitations of metal-based motors for biomedical applications.[63] Polymer-based nanomotors offer distinct advantages over metal-based counterparts, particularly in terms of biocompatibility, biodegradability, and molecular tunability.[63] Unlike rigid metal nanomotors, polymer nanomotors can be designed with flexible, stimuli-responsive properties, enabling precise control over motion, drug release, and environmental interactions.[48] The ability to self-assembly into vesicular structure allows polymersome nanomotors for dual cargo encapsulation (both hydrophilic and hydrophobic), which is challenging for metal-based systems.[24,64–66] In addition, compared with lipid-based nanomotors, which often suffer from structural instability and limited cargo encapsulation capacity, polymersomes provide superior mechanical robustness and stable membrane properties for enhanced functionality.[67,68] These architectures therefore enable the engineering of multifunctional nanomotors that can carry out several tasks simultaneously, including imaging, targeting, and treatment.[69,70] Additionally, polymer nanomotors can avoid toxicity concerns associated with heavy metals, making them more suitable for biomedical applications, including targeted drug delivery and *in vivo* therapeutic interventions.[63]

In addition to the above merits, polymersomes also provide a versatile platform for nanomotor design due to their soft, flexible nature and ability to undergo shape transformations, such as sphere-to-stomatocyte or sphere-to-tubule transitions under external stimuli.[71–74] These shape transformations are usually required to construct anisotropic scaffolds.[65] Polymersome-based nanomotors therefore offer a promising solution for overcoming the limitations of traditional delivery systems.[48,75] Polymersomes can be tailored for various biomedical applications, including targeted drug delivery to tumors or stimuli-responsive drug release.[76] For instance, the surface chemistry of polymersomes can be easily modified with ligands, antibodies, or targeting molecules, enhancing their ability to interact specifically with target cells or tissues.[70] Additionally, these polymersome nanomotors can be engineered with elements that are responsive to light, pH, temperature, or enzymatic triggers. This enables controlled motion and the precise release of therapeutic agents, enhancing their potential in nanomedicine.[48,77–79] The integration of autonomous motion into polymersomes is a promising strategy to enhance precision in drug delivery, overcoming challenges like limited penetration in tissues or poor targeting to diseased cells.[80–84] These systems can respond to environmental cues (pH, enzymes, or other stimuli), self-propel, and navigate toward specific locations, providing an alternative to passive delivery systems that rely on blood circulation or diffusion to reach target areas.[85,86] This concept is particularly relevant in areas like cancer therapy and precision medicine, where active targeting can significantly improve treatment efficacy.[87] Polymersome-based nanomotors with adaptive and dynamic features are therefore represented as an alternative platform for delivery systems in nanomedicine. In this perspective, we highlight recent development in the design and construction of polymersome-based nanomotors as promising delivery vehicles in nanomedicine (Scheme 1). We will start with illustrating the strategies of polymersome-based shape transformations. This is essential to create anisotropic vehicles that allow to integrate motile features, of which some specific examples will be highlighted. Next, methods and approaches for realizing active motion and motion control of polymer nanomotors, such as speed, direction and dynamic regulation, will be presented. Then the potential utility of polymersome-based nanomotors in

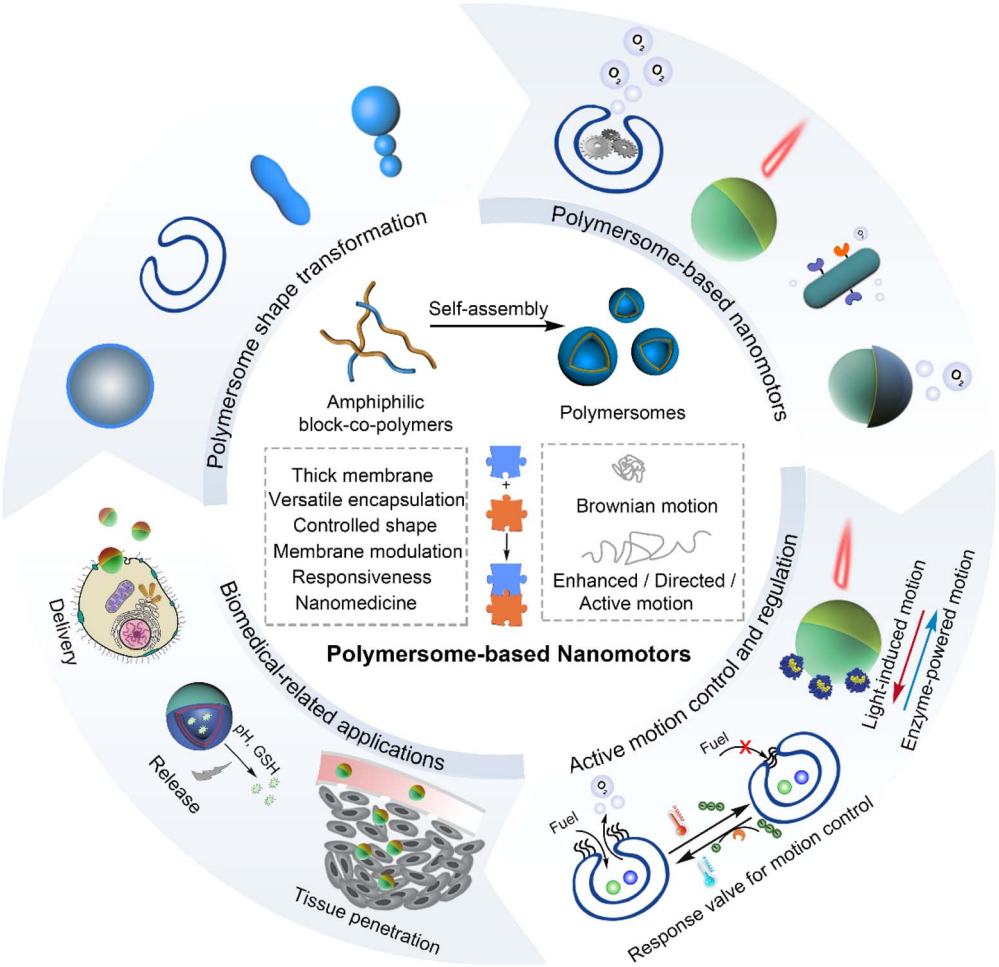

Scheme 1 Schematic illustration of shape transformation of polymersomes and polymersome-based nanomotors for diverse biomedical-related applications.

the biomedical field will be discussed. We will end with a perspective on how active motion and polymeric-based self-assemblies could be synergistically merged for generating adaptive, active, and functional delivery systems in biomedical fields.

Polymersome-based nanomotors

A fundamental requirement in the design of nanomotors is that the platform's structure must generate a higher net force on one side, typically achieved by engineering anisotropic scaffolds or asymmetrically distributing active moieties on the surface.[55,88,89] While lipid-based structures can undergo complex shape changes in response to environmental stimuli, these transformations often occur on very short time scales, making it challenging to study their mechanisms or kinetically trap these intermediate shapes for structural investigations and applications. In contrast, polymersomes possess thicker membranes due to the high molecular weight of the polymer chains.[23] This confers mechanical stability, enabling a broader range of potential curvatures and stress tolerance, allowing polymersomes to be converted between different shapes without compromising structural integrity—which is ideal for nanomotor fabrication.[65] The design of polymersome-based nanomotors integrates several key principles, including morphology engineering to exploit the structural flexibility of polymersomes, the strategic incorporation of catalytic components for propulsion, and precise control over active motion.[90–92] These aspects make polymersomes a robust and adaptable platform for engineering nanomotors capable of efficient navigation and function in complex biological environments.

Shape transformation of polymersomes

One of the typical strategies in engineering polymersome nanomotors is utilizing a shape transformation approach to engineer asymmetric polymersomes to meet the fundamental requirement of motor design.[65] Polymersomes are usually spherical morphologies due to the minimized interfacial tension, while they can transform into more anisotropic shapes, such as rods, tubules, or elongated structures.[93,94] The morphology transformation behavior of polymersomes is usually dictated by a polymer architecture-driven transformation or external stimuli-driven morphology change.[95,96] Both approaches leverage the inherent flexibility of polymeric

materials to induce changes in shape, providing a dynamic means of controlling the behavior and function of polymersomes.[97,98] Morphology engineering of polymersomes towards shape transformations is closely associated with the self-assembly behavior of copolymers, which is inextricably constrained and dictated by hydrophilic/hydrophobic ratios, membrane curvature, geometric, polymer chain entropy effects (relating to the packing parameter), and other kinetic factors.[99] It is strongly correlated to the polymer compositions, preparation methods, environmental conditions, and external triggers. Generally, polymersomes are self-assembled from amphiphilic BCPs with a hydrophilic fraction between 0.25 and 0.45.[100,101] An increased portion in the hydrophilic part usually yields micellar or worm-like structures due to the extended hydration and increased surface curvature.[102–106] Adjusting the hydrophobic/hydrophilic ratio in the chemical design or by environmental stimuli is a direct approach to dictate the self-assembly behavior of BCPs, thereby affecting the properties of the polymersomes (*e.g.*, size, morphology, membrane permeability).[107–110] Representative examples are given by the groups of Yan, Liu, Voit, Bruns, and Arms in which various stimuli (*e.g.*, pH, CO_2, glutathione (GSH)) and external triggers (mainly light) are utilized to precisely manipulate the size and properties of the hydrophobic blocks.[110–114] This usually induces a re-arrangement of polymeric chains, accompanied by the physical–chemical properties change of the self-assemblies, also including morphology transformations of polymersomes.[98,115] For instance, Yan and co-workers introduced a class of gas-responsive polymersome systems from cyanine-containing block copolymers, poly(ethylene oxide)-poly((2-hydroxyphenyl cyanine) ethylmethacrylate) (PEO-*b*-PCy) (Fig. 1a).[116] Upon the intake of SO_2 gas, the tautomerism of the cyanine groups endowed the polymer with a highly sensitive, reversible, and exclusive response, driving the deformation of spherical polymersomes into long nanotubes. The morphology transformation was realized *via* axial stretching and anisotropic extrusion of the membranes, switching the molecular membrane interaction from π–π stacking (before SO_2 exposure) to hydrogen bonding (after SO_2 exposure), which governs the membrane's structural changes. Molecular response *via* breathing SO_2 induced a subtle polymer structural conversion, which resulted in a large transition and remodeling of the membrane geometry, yielding the formation of tubesomes. In addition, the degree of membrane 1D stretching was also well-regulated by the amount of SO_2, allowing selective transmembrane transfer of various sizes of cargo. For instance, small (5-dFu), medium (FITC-gal), and large (TR-dextran) molecules exhibited distinct release profiles depending on SO_2 concentrations. Small cargoes can escape polymer membranes at lower SO_2 levels, while larger ones require higher concentrations of SO_2, mimicking biological membrane behavior.

Membrane crosslinking is recognized as another alternative approach to induce polymersome shape transformation from a chemical-responsive perspective. For instance, van Oers *et al.* demonstrated that polymersomes from poly(ethylene glycol)-*b*-poly(styrene-*co*-4-vinylbenzylazide) (PEG_{44}-*b*-P(S-*co*-4-VBA), underwent a shape transformation from spherical to tubular in response to a cross-linking reaction (Fig. 1b).[117] This transformation is driven by a strain-promoted alkyne–azide cycloaddition (SPAAC) reaction between azide handles within the hydrophobic domain of the polymersome membrane and a bicyclo[6.1.0]nonyne (BCN) cross-linker. The process caused the vesicles to stretch in one dimension, forming tubular structures. The concentration and nature of the cross-linker significantly affected the extent of the shape transformation. A BCN-to-azide ratio of 1 : 1 resulted in polymersomes retaining their spherical morphology, but increasing the cross-linker concentration to a 2 : 1 or higher ratio induced a progressive elongation, eventually yielding tubular polymersomes up to 2 μm in length. In addition, the introduction of a cleavable cross-linker with a disulfide bridge enabled reversible shape transformation. When the disulfide bond was cleaved, the polymersomes returned to their original spherical shape, demonstrating that the shape transformation is kinetically

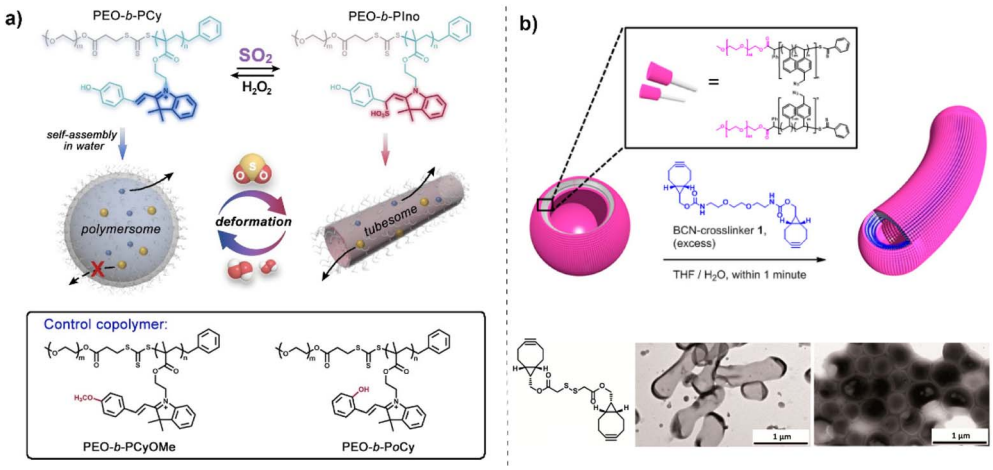

Fig. 1 (a) SO_2 gas-driven deformation behavior of PEO-*b*-PCy polymersomes in aqueous solution into tubesomes. Reproduced with permission from (ref. 116). Copyright 2023 Wiley-VCH. (b) Crosslinking-induced deformation of PEG-PS polymersomes into a tubular shape, which can be reversible upon the use of a disulfide crosslinker. Reproduced with permission from (ref. 117). Copyright 2013 America Chemical Society.

controlled and can be manipulated for potential applications. The shape transformation is in this case not a result of osmosis or fusion but is linked to the introduction of asymmetry in cross-linking density across the polymersome membrane. This gradient creates spontaneous curvature and tension within the bilayer, leading to one-dimensional stretching.

For the polymersome assemblies that did not contain chemical groups in response to external triggers, their shape transformation processes are usually realized *via* manipulating the properties of the polymersome membrane (*e.g.*, tension, fusion, curvature, directional interactions).[71] Directional aromatic interactions within the polymersome membrane can be harnessed to create non-spherical polymersomes. For instance, Thordarson and co-workers presented an approach to fabricating non-spherical polymersomes with anisotropic membranes from perylene-bearing diblock-*co*-polymer poly(ethylene glycol)-*b*-poly(*N*-isopropylacrylamide-*co*-perylene diester monoamide (PEG_{43}-*b*-P($NIPAM_{21}$-*co*-$PDMI_9$)) (Fig. 2a).[118] By exploiting directional aromatic interactions between perylene units within the polymersome membrane, they were able to generate ellipsoidal and tubular-shaped polymersomes. The shape transformation was achieved by controlling the solvation and desolvation of the aromatic side chains through adjustments in solvent composition, specifically using tetrahydrofuran (THF) and water mixtures. The incorporation of perylene side chains in the polymer introduced strong hydrophobic and directional aromatic (π–π) stacking interactions. These interactions played a critical role in driving the self-assembly of the polymersomes into non-spherical shapes. The strength of aromatic interactions decreased as the solvent composition changed from THF to water, leading to different degrees of membrane tension and curvature, which ultimately dictates the final shape of the polymersomes. The authors were able to identify five distinct aggregate morphologies, including small ellipsoidal micelles, medium ellipsoidal polymersomes, large ellipsoidal polymersomes, giant ellipsoidal polymersomes, and tubular polymersomes by varying the THF-to-water ratio during the self-assembly process. The membrane thickness of the polymersomes was found to vary with the size and shape of the aggregates. Smaller ellipsoidal structures exhibited thinner membranes, while tubular polymersomes had significantly thicker membranes. This variation is attributed to the degree of aromatic stacking and the packing arrangement of the polymer chains within the membrane. Control experiments with polymers containing different amounts of perylene showed that the aromatic content is crucial for the formation of non-spherical polymersomes. Polymers with reduced aromatic content failed to form vesicles and instead formed micelles, highlighting the importance of aromatic interactions in driving the formation of anisotropic structures. These findings contribute significantly to the understanding of how directional aromatic interactions can be harnessed to create non-spherical polymersomes with potential applications in material science and nanomedicine.

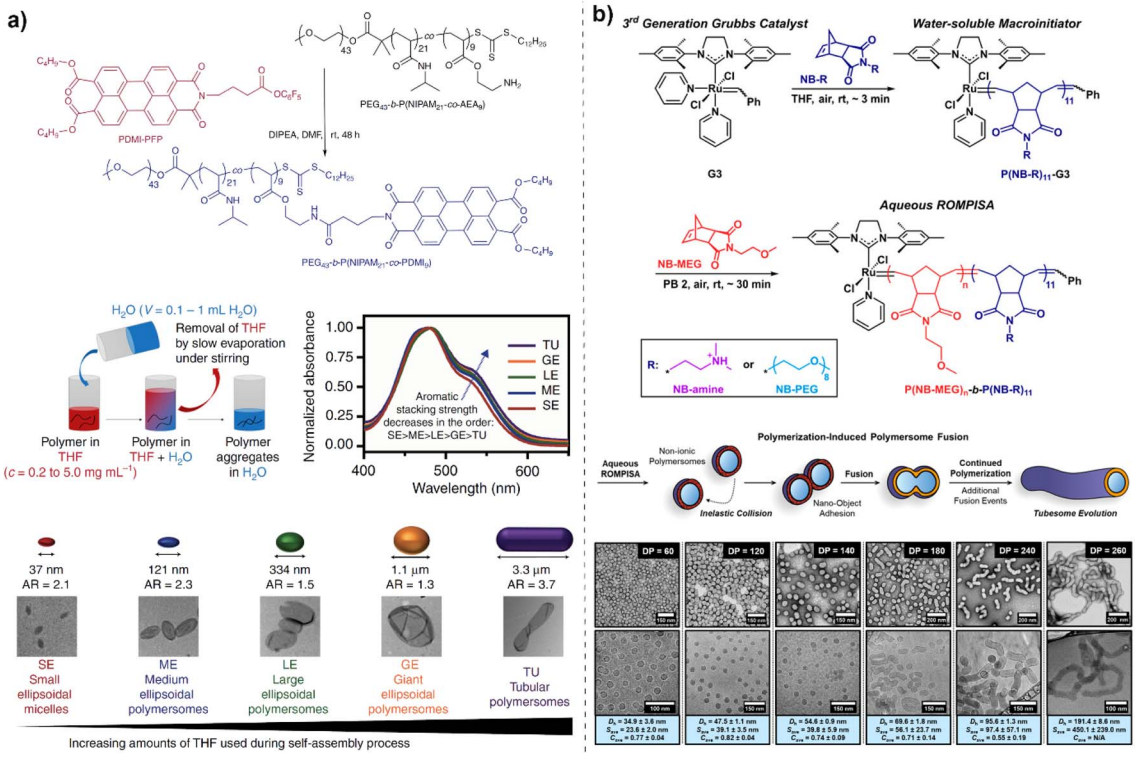

Fig. 2 (a) *Via* controlling the solvation and desolvation of the aromatic side chains through adjustments in solvent composition, specifically using tetrahydrofuran (THF) and water mixtures, different morphologies of polymersomes were obtained which displayed varied absorption spectra. Reproduced with permission from (ref. 118). Copyright 2017 Springer Nature. (b) Polymerization-induced fusion of polymersomes, wherein spherical polymersomes fuse into anisotropic tubular polymersomes (tubesomes) during polymerization. Reproduced with permission from (ref. 119). Copyright 2019 America Chemical Society.

Membrane tension is identified as a critical factor driving the fusion of polymersomes, with higher tension correlating with increased bending energy. The properties of the core block of BCPs significantly affect the membrane bending behaviors, thereby dictating the vesicle morphology. For instance, O'Reilly and co-workers introduced the concept of polymerization-induced fusion of polymersomes, wherein spherical polymersomes fused into anisotropic tubular polymersomes (tubesomes) during polymerization (Fig. 2b).[119] This phenomenon occurred without the need for external forces, driven by membrane tension built up during the polymerization process. The fusion process occurred through a step-growth mechanism where spherical polymersomes merge, confirmed by Förster resonance energy transfer (FRET) studies and confocal microscopy. Membrane tension played a significant role in initiating the fusion, and this tension was exerted by the growing polymer chains during the aqueous ring-opening metathesis polymerization-induced self-assembly (ROMPISA) process. The final tubesome morphology could be controlled by varying the degree of polymerization (DP) of the core-forming polymer block. The study demonstrates that targeting different DPs allows for control over the length distribution of the tubesomes and larger DPs promote the development of longer tubesomes. The ROMPISA process is demonstrated to be an efficient, one-pot synthesis method that allows for precise control over polymersome morphology. The study emphasizes the ability to generate mixtures of spherical and tubular polymersomes or pure tubesomes under controlled conditions, representing a significant advancement in polymersome engineering.

The polymer addition/insertion approach is another facile methodology for manipulating shape change in polymersomes.[120] Wilson and co-workers used this method to construct asymmetrical polymersomes with distinct morphologies.[121,122] The shape transformation was realized *via* combining osmotic change, controlled fusion, or manipulating membrane curvature procedures *via* chemical addition. For instance, the addition of a trace amount of PEG (0.005 wt%) in the poly(ethylene glycol)-*block*-polystyrene (PEG-*b*-PS) based polymersome aqueous solution together with a mixture of THF and dioxane (~77% volume ratio) led to the polymersome shape transformation (Fig. 3).[123] The addition of trace PEG under nonequilibrium conditions of PEG-*b*-PS assembly pushed further the polymersome transformation beyond the low-energy-state, which allows for tailored control over a wide array of morphologies. In a very short time, polymersomes with distinct morphologies including spheres, ellipsoids, tubes, discs, stomatocytes, and complex nested structures like stomatocyte-in-stomatocyte and disc-in-disc vesicles were formed. The different morphologies were correlated to the PEG concentration and water content, which affected the shape transformations driven primarily by osmotic pressure dynamics and PEG's dual role in enhancing membrane rigidity and reducing permeability. Their findings reveal that the addition of

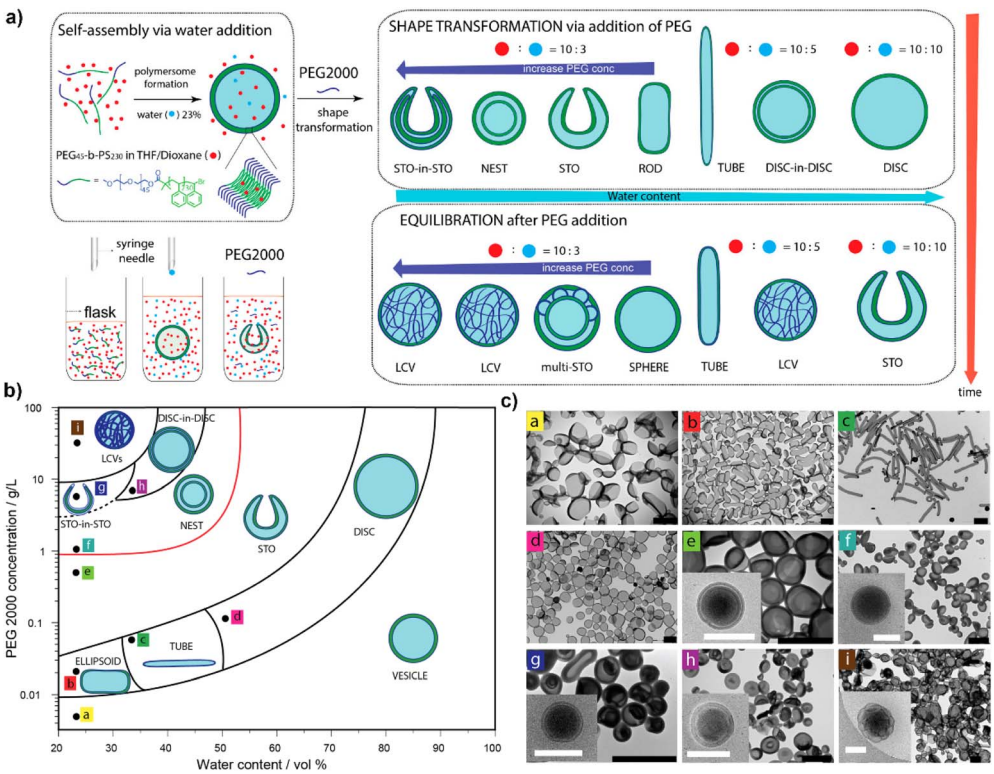

Fig. 3 (a) The addition of a trace amount of PEG in the poly(ethylene glycol)-*block*-polystyrene (PEG-*b*-PS) based polymersome solution together with a mixture of THF and dioxane leads to the polymersome shape transformation; (b) phase diagram of polymersome morphologies before equilibrium; (c) TEM and cryo-TEM images of various polymersome morphologies. Reproduced with permission from (ref. 123). Copyright 2019 America Chemical Society.

water increases osmotic pressure, pushing the polymersomes out of equilibrium, while PEG acts as a fusogen, facilitating both the shape transition and the stabilization of unique morphologies through kinetic trapping. The shape transformation of PEG-PS polymersomes can also be realized *via* the addition of responsive polymers such as poly(*N*-isopropylacrylamide) (PNIPAm). The transition of PNIPAm from a hydrophilic to a hydrophobic state resulted in a change in the curvature of the polymersome membrane, leading to non-asymmetric shapes such as tentacle, cigar, boomerang, and starfish-like structures. In addition, increased solvent addition led to the dissociation of PNIPAm and return to native polymersome shapes, shedding light on dynamic membrane adaptations. These studies present alternative approaches to morphology engineering with polymersomes, showing how dynamic polymer interactions can effectively generate and modulate membrane curvature toward the formation of asymmetrical polymersomes.

Constructing polymersome nanomotors

By carefully designing the molecular structure of the amphiphilic BCPs, polymersomes in solution can be created to adapt different shapes under specific conditions, creating asymmetrical architectures for nanomotor engineering.[65] A prerequisite for the shape transformation is the fluidity of the polymersome membrane, inducing the chain rearrangement to allow a morphology change.[71] This is usually achieved upon the increase of the environmental temperature to that above the polymer glass transition temperature. A more convenient approach to improve the membrane dynamicity of polymersomes is the use of a plasticizing agent (usually organic solvent), which makes the glass–rubbery transition occur at or even below ambient conditions.[94] Importantly, the plasticizing agent can be simply removed *via* dialysis or quenched by adding aqueous solutions. This allows facile control of the morphology transformation process and kinetically trapping the desired shape. Van Hest's group played a pioneering role in the control of polymersome shape transformation and engineering polymersome nanomotors.[90–92] They presented an osmotic pressure-based approach to induce the morphology control from spherical polymersomes into stomatocytes (*i.e.*, bowl-shaped polymersomes), as a useful platform for nanomotor preparation. This was generally realized by firstly preparing spherical polymersomes in a mixture of organic solvent (for solvation and as a plasticizing agent) and water. Then the non-spherical

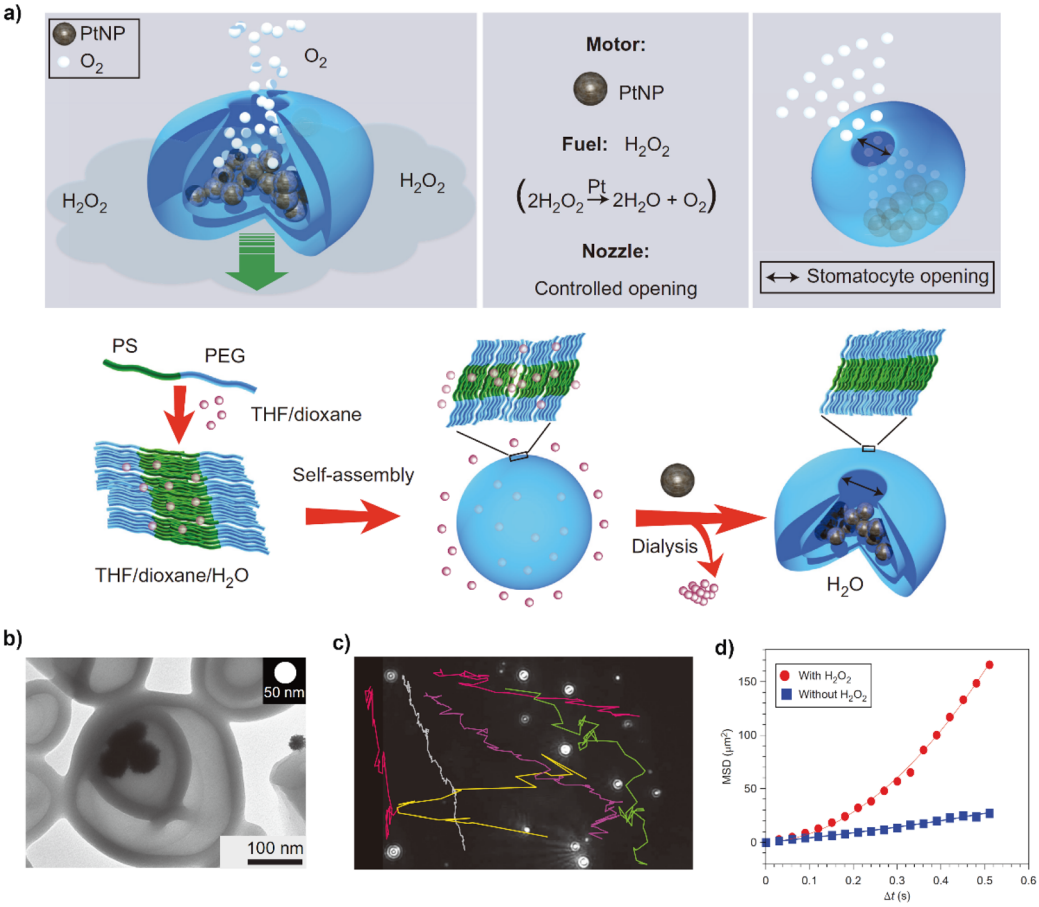

Fig. 4 (a) PEG-PS polymersomes displayed shape transformation into stomatocytes which allowed trapping of active catalytic Pt particles. (b) TEM image of Pt nanoparticles encapsulated in stomatocytes. (c) Motion trajectories of the stomatocyte nanomotors. (d) MSD profile of stomatocyte nanomotors with and without H_2O_2. Reproduced with permission from (ref. 92). Copyright 2012 Springer Nature.

polymersomes were prepared *via* a dialysis procedure induced osmotic shock, shape deformation, and kinetic trapping. For instance, spherical polymersomes from poly(ethylene glycol)-*b*-poly(styrene) (PEG-*b*-PS) were prepared first *via* a well-established solvent-switch method. The polymersomes displayed a dynamic shape because of the fluidity of the hydrophobic block in the mixture of organic solution (usually THF and 1,4-dioxane) and water (50% volume ratio) (Fig. 4).[92] Upon dialysis, the rapid diffusion of the organic solvent into the bulky dialysis solution caused the membrane component (hydrophobic polystyrene) to lose its fluidity and recover into a glass state. This reduced the membrane permeability and hindered the reversal transport of water molecules into the polymersomes, which generated an osmotic pressure. The non-equilibrium osmotic conditions in and out of the polymersomes induced the folding of the hydrophobic membrane and the formation of stomatocytes. Importantly, the formation of the polymersome stomatocytes enabled the encapsulation of catalytic machinery such as Pt nanoparticles or enzymes (*e.g.*, glucose oxidase, catalase) in the newly formed cavity. The presence of an open-neck structure allowed for facile accessibility of the environmental fuels (*e.g.*, glucose, H_2O_2) and expulsion of gas molecules, thereby propelling the polymersomes in the opposite direction of the open neck.

The osmotic pressure-induced morphology engineering can also be applied to polymersomes from poly(ethylene glycol)-*b*-poly(D, L-lactide) (PEG-*b*-PDLLA).[94,124] The non-biodegradability of PEG-PS co-polymers limits their further exploration in biomedical applications, although engineering hybrid polymeric systems *via* blending with poly(ethylene glycol)-*b*-poly(-caprolactone) (PEG-PCL) can impart partial degradability and drug release features.[125] PEG-*b*-PDLLA co-polymers are more desired to be explored for the formation of polymersome nanomotors with inherent biodegradability. PEG-*b*-PDLLA polymersomes displayed a powerful ability towards controlled shape transformation into various morphologies including spheroids, discs, stomatocytes, and tubes.[94,124,126,127] For instance, PEG-PDLLA polymersomes with surface 5% azide handles, upon dialysis under hypertonic conditions, transformed into tubular structures (Fig. 5a).[126] Upon further surface modification with catalase (*via* click-chemistry mediated conjugation), the polymeric nanotubes displayed active motion in the presence of hydrogen peroxide (H_2O_2). Compared with spherical delivery systems, the tubular-like morphology is recognized to have potential advantages in terms of reduced nonspecific adhesion to cells and a higher ability to interact with the immune system. Upon integration with targeting ligands, these nanotubes have a high possibility to boost the delivery efficiency and enhance cellular uptake.

The shape feature of polymersomes and their morphology engineering can also be realized by creating asymmetry in the polymersome bilayer, where the inner and outer layers consist of different block copolymers or have distinct hydrophobic/hydrophilic balances, inducing spontaneous shape transformations. This asymmetry creates natural curvature within the membrane, facilitating the formation of polymersomes with unique shapes, which can be utilized for motor design and propulsion behaviors. Upon integration with an engine, the non-spherical polymersomes allow for directed motion, as the nanomotor's geometry helps convert chemical or physical energy into mechanical movement more effectively than spherical structures. For instance, Battaglia and co-workers

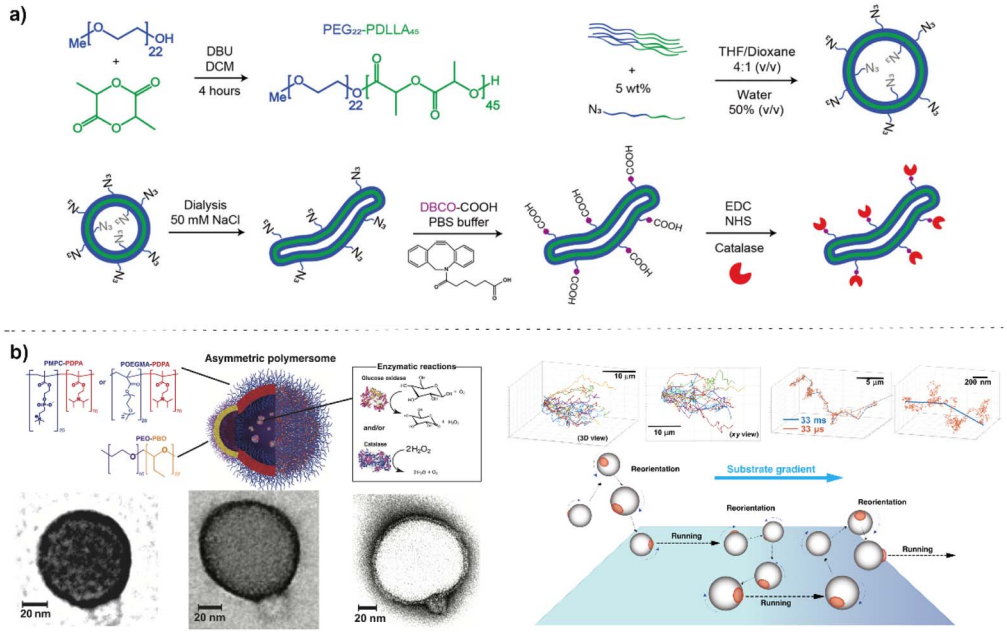

Fig. 5 (a) PEG-PDLLA polymersomes upon dialysis under hypertonic conditions, transformed into a tubular structure, which allowed conjugation with catalase and engineering into active nanomotors. Reproduced with permission from (ref. 126). Copyright 2018, Royal Society of Chemistry. (b) Blending block-co-polymers with distinct compositions for the formation of polymersomes with asymmetric membranes, which displayed active motility in the presence of fuel. Reproduced with permission from (ref. 128). Copyright 2017, AAAS.

reported a self-assembled polymeric nanomotor *via* mixing two types of block copolymers including poly(ethylene oxide)–poly(butylene oxide) (PEO–PBO) and poly(-methacryloxyphosphorylcholine)–poly(diisopropylaminoethyl methacrylate) (PMPC–PDPA) or poly(oligo ethylene glycol methyl ether methacrylate)–poly(diisopropylamino ethyl methacrylate) (POEGMA–PDPA) (Fig. 5b).[128] Blending block-copolymers with distinct compositions in the formation of polymersomes is a viable approach to create asymmetry in the membrane. Initially, the mixture of polymers self-assembled into spherical vesicles. With prolonged incubation, a phase-separation process within the membrane occurred between the PEO–PBO and the PDPA–POEGMA/PMPC copolymers, resulting in the formation of a small PEO–PBO bulge because of the incompatibility of the different types of polymers. Enzymes that can perform cascade reactions such as glucose oxidase and catalase were encapsulated inside the asymmetric polymersomes. The environmental fuel (*i.e.*, glucose) and reaction products diffused more easily through the more permeable PEO–PBO patch. In this way, a concentration gradient of products was formed, which resulted in a slip velocity leading to active motion. In addition, the asymmetric polymersomes displayed chemotactic behaviors, in which the movement of polymersomes was in the direction of an increasing concentration of substrate.

Another widely utilized approach to fabricating asymmetrical architectures for nanomotor engineering is the sputter-coating approach on the surface of spherical particles.[38,129,130] It typically involves the deposition of a particle solution, drying, coating, and recovery in the fabrication procedure. Usually, Pt or Au shells are deposited as a hemispherical shell on the particle surface.[48,67] A Janus structure is then created that has distinct physical or chemical properties on each side, which is crucial for propulsion mechanisms in nanomotors. For instance, a spherical particle partially coated with platinum (acting as a catalyst) can propel itself in a hydrogen peroxide solution due to an asymmetric chemical reaction releasing a local gas that propels the motor forward.[131,132] The asymmetrical distribution of catalytic particles ensures directed propulsion, as the generated gas or chemical gradient results in a directional push.[133] Sputter-coating can be used with different materials that show solid and rigid features, including metals, SiO_2, and $CaCO_3$ particles, and particle functionalization approaches such as layer-by-layer self-assembly are usually involved during nanomotor fabrication.[134,135] The flexibility in particle design allows tailored interfacial engineering, rendering key features toward a broad range of applications in fields such as biomedical engineering, environmental monitoring, and microfluidics.[136–139] Janus polymeric motors with an Au coating and surface erythrocyte membrane modification, as an example, served as near-infrared (NIR) laser-powered motors specifically designed for active drug delivery and thrombus therapy.[58] The sputter coating approach was also applied in the fabricating of polymersome nanomotors. Peng *et al.*, presented the design and construction of Janus polymersome nanomotors from amphiphilic block copolymers (poly(ethylene glycol)-*b*-polystyrene and poly(acrylic acid)-*b*-polystyrene) *via* a solvent switch method and post-sputter-coating approach (Fig. 6).[67] The nanomotors were equipped with a platinum cap to enable propulsion powered by hydrogen peroxide. The design allowed

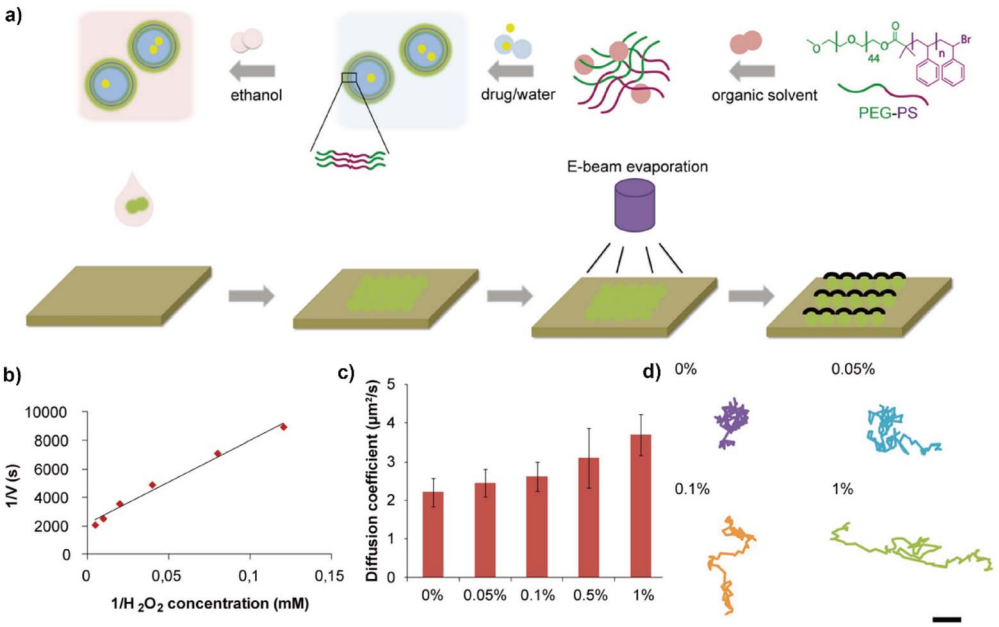

Fig. 6 (a) The design and construction of Janus polymersome nanomotors from amphiphilic block copolymers (poly(ethylene glycol)-*b*-polystyrene and poly(acrylic acid)-*b*-polystyrene) *via* a solvent switch method and post sputter coating approach; (b) Lineweaver–Burk plot for the hydrogen peroxide substrate; (c) average diffusion coefficient of polymersome nanomotors at different concentrations of hydrogen peroxide; (d) typical tracking paths of polymersome nanomotors at different concentrations of hydrogen peroxide. Reproduced with permission from (ref. 67). Copyright 2023 Wiley-VCH.

for tunable size (100 to 300 nm) and high cargo (fluorescein sodium) loading capacity. Upon ultrasound treatment, the integrity of the polymersome nanomotor structure was compromised. This resulted in cargo release, displaying potential for controlled release in response to external triggers. While sputter coating works well for small-scale experiments, scaling up the process to industrial levels with high uniformity and precision across many particles can be challenging. In addition, sputter coating is usually only compatible with rigid materials that can survive during the harsh fabrication process. This limits its applicability with soft polymersomes, as their structure, integrity, cargo loading, and morphology could be highly affected due to mechanical and chemical stresses involved. Surface roughness or imperfections could arise during the sputter coating process, particularly if the coating material does not adhere uniformly or if environmental conditions fluctuate during fabrication. The generation of asymmetrical polymersomes in solution for nanomotor fabrication would be a more desirable alternative, especially for applications that require the preservation of their key properties.

Spatial distribution of catalytic engine

Polymersome stomatocytes are considered effective scaffolds to encapsulate catalytic engines to induce motion, however, it is challenging to control the neck size.[79] This can be most effectively achieved for PEG-PS polymersome-based stomatocytes, but their non-biocompatible and non-biodegradable features severely limit their application in biomedicine-related fields. For the polymersome stomatocytes from biodegradable PEG-PDLLA, their neck size is found usually bigger than 30 nm, which is not optimal for retaining catalytic nanoparticles or enzymes. Considering the small size of the catalyst (usually around or below 10 nm), it is very easy for them to diffuse out from the stomatocyte lumen to the bulk solution. This makes the long-term operation of these stomatocyte nanomotors a challenge. Several promising strategies have been presented to address this challenge. For instance, Toebes *et al.*, introduced an approach to creating biodegradable polymeric nanomotors with a multivalent design, specifically using PEG-PDLLA stomatocytes (Fig. 7).[127] They first blended azide-tagged PEG-PDLLA with normal PEG_{22}-$PDLLA_{90}$ and PEG_{44}-$PDLLA_{90}$ for the formation of polymersomes in a solvent (THF/dioxane) and water system. Dialysis against a 10 mM NaCl solution promoted the formation of stomatocytes, which are bowl-shaped vesicles with an open neck (size ~30 nm). The outer azide handles on the stomatocytes were selectively reduced into amine groups using tris(2-carboxyethyl)phosphine (TCEP) immobilized beads. This selective reduction allowed the maintenance of azide functionalization in the inner cavity of stomatocytes, which was then coupled with DBCO-functionalized catalase and glucose oxidase through strain-promoted azide–alkyne cycloaddition. The covalent linkage and spatial control of the catalyst prevented leakage of the enzymes and led to a self-propelling mechanism when glucose was present. The motility of the nanomotors was tested by adding physiological concentrations of glucose or hydrogen peroxide and observing their movement *via* microscopy using various fuel concentrations. The observed motion profiles of the enzyme-functionalized stomatocytes were consistent with a bubble propulsion mechanism. This method enhances the reproducibility and efficiency of enzyme incorporation.

In situ formation of relatively large particle clusters in the cavity of polymersome stomatocytes is another viable approach to trap catalytic particles. For instance, the enzymes catalase and glucose oxidase inside PEG-PS stomatocytes can be cross-linked with genipin under mild conditions.[140] A similar strategy can also be applied to PEG-PDLLA-based polymersome stomatocytes. Pijpers *et al.* presented an alternative approach to engineering biodegradable hybrid nanomotors using a compartmentalized synthesis of inorganic manganese dioxide (MnO_2) nanoparticles within stomatocyte structures (Fig. 8a).[141–143] Manganese dioxide nanoparticles were synthesized inside the stomatocyte cavities by dissolving potassium permanganate ($KMnO_4$) followed by reduction with sodium

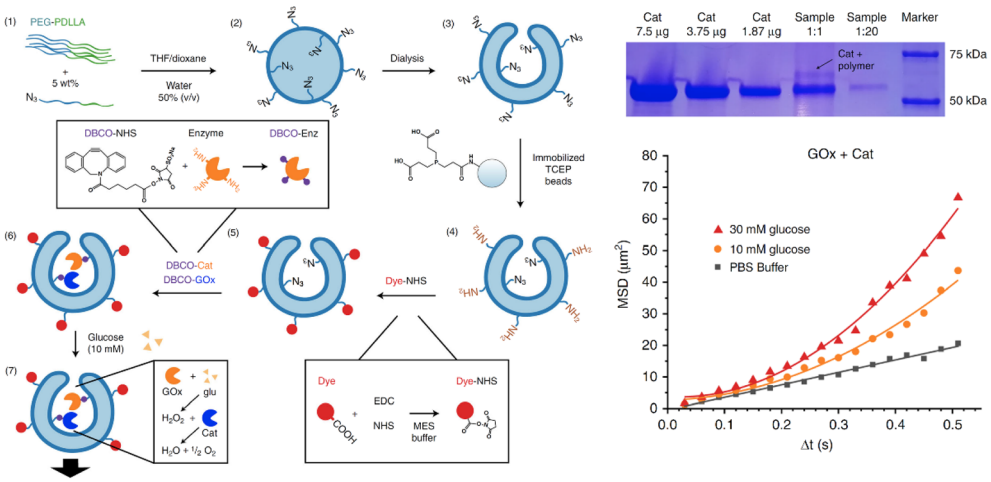

Fig. 7 Biodegradable polymeric nanomotors with a multivalent design, specifically using PEG-PDLLA stomatocytes with spatial control over catalyst, allowed selective conjugation of active enzymes inside the cavity of stomatocytes. Upon the presence of fuels, the stomatocytes displayed motility. Reproduced with permission from (ref. 127). Copyright 2019 Springer Nature.

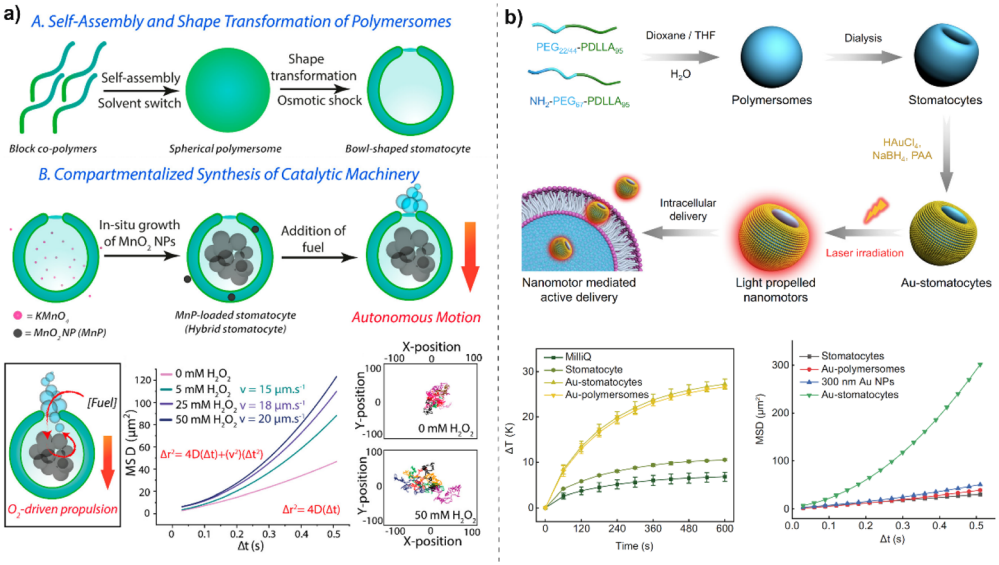

Fig. 8 (a) Engineering biodegradable hybrid nanomotors using a compartmentalized synthesis of inorganic manganese dioxide (MnO_2) nanoparticles within stomatocyte structures, which showed increased velocity upon increasing concentrations of H_2O_2. Reproduced with permission from (ref. 141). Copyright 2020 America Chemical Society. (b) Biodegradable PEG-PDLLA bowl-shaped polymersomes (stomatocytes) modified with gold nanoparticles (Au NPs) to create light-activated nanomotors, which exhibit controllable motion with remarkable velocities. Reproduced with permission from (ref. 145). Copyright 2024 Springer Nature.

thiosulfate ($Na_2S_2O_3$). Bovine serum albumin (BSA) was used for stabilization, limiting uncontrolled particle aggregation. The internal structure and size distribution of MnO_2 nanoparticles within the stomatocytes were characterized using cryogenic transmission electron microscopy (cryo-TEM) and three-dimensional tomographic reconstruction. The MnO_2 nanoparticles acted like a nanoenzyme, which can convert hydrogen peroxide (H_2O_2) into gas nanobubbles, inducing motion (tracked *via* nanoparticle tracking analysis (NTA)).[143,144] This approach also ensured stability against proteolytic degradation that typically affects enzymatically powered nanomotors. These hybrid nanomotors demonstrated effective autonomous motion in biological settings while maintaining good cell viability, suggesting their potential for various biomedical applications, including drug delivery and cancer therapy.

Via adopting a similar concept of *in situ* nanoparticle synthesis, Wang *et al.* introduced biodegradable PEG-PDLLA stomatocytes modified with gold nanoparticles (Au NPs) to create light-activated nanomotors, which exhibit controllable motion with remarkable velocities of up to 125 μm s^{-1} (Fig. 8b).[145] Gold nanoparticles were *in situ* synthesized onto the surface of stomatocytes assisted by non-covalent binding, creating Au-stomatocytes. Cryogenic Electron Microscopy (Cryo-TEM) and Cryo-Electron Tomography (Cryo-ET) were employed to confirm the morphology and spatial distribution of Au NPs on the stomatocyte surface. The photothermal effect of the Au-stomatocytes was assessed by measuring temperature changes upon laser irradiation (660 nm), establishing the relationship between the concentration of Au-stomatocytes and temperature increase. The fast motion is attributed to the nonuniform distribution of Au NPs along the *z*-axis on the stomatocyte surface, which leads to a spatial temperature gradient when exposed to laser light. This localized heating enhances the photothermal effect, enabling efficient propulsion through thermophoresis. The Au-stomatocytes demonstrated good stability under laser irradiation and maintained their function in different media (pure water, PBS, DMEM). They showed minimal cytotoxicity at tested concentrations, indicating potential for safe application in biomedical settings. Additionally, the high motility of these nanomotors in biological environments signifies their potential use in targeted drug delivery systems.

Besides stomatocytes, polymersomes can be shaped in different topologies that are suitable for nanomotor development. Cao *et al.* presented the design and preparation of aggregation-induced emission (AIE) polymersomes with cucurbit-like morphology, which exhibited enzyme-mediated motility (Fig. 9).[146] They synthesized amphiphilic block copolymers containing both poly(ethylene glycol) (PEG) and AIE blocks (PEG-PAIE) *via* ring-opening polymerizations and post-functionalization. The AIE moieties provide robust fluorescence, overcoming conventional issues such as low fluorescence, photobleaching, and leakage, making these structures promising for biomedical applications in imaging and tracking.[147–150] The self-assembly of these polymers into spherical AIE-polymersomes was realized using a solvent switch method, followed by dialysis to remove organic solvents. The morphology of the polymersomes was manipulated by varying the concentration of NaCl during dialysis. This adjustment facilitated the transition from spherical to cucurbit shapes through osmotically induced shape transformation, confirmed *via* cryo-TEM. Then the layer-by-layer assembly technique was employed for integrating enzyme machinery such as urease and catalase onto the surface of the cucurbit-shaped AIE-

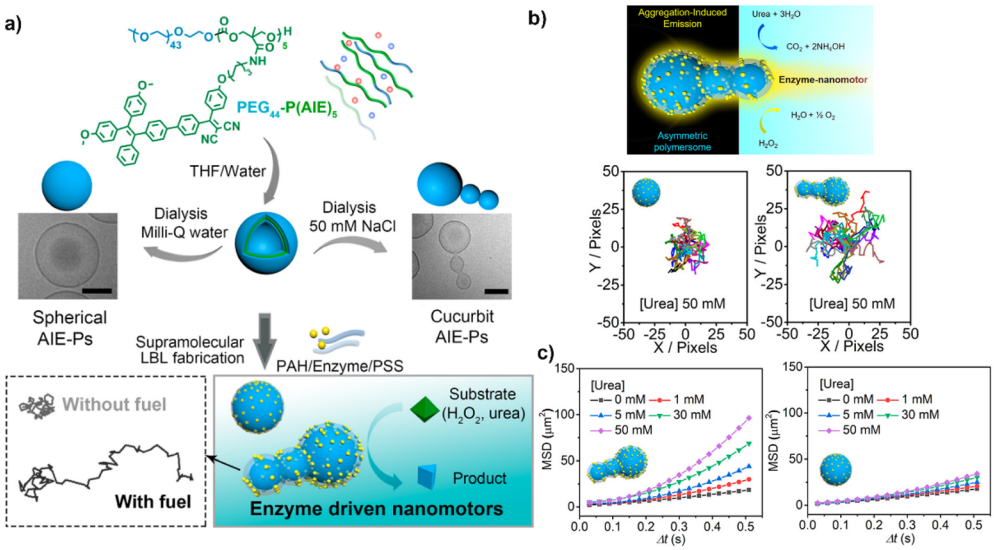

Fig. 9 (a) The design and preparation of aggregation-induced emission (AIE) polymersomes with cucurbit-like morphology. Upon LBL interfacial assembly, enzymes are displayed on the polymersome surface. (b) Cucurbit polymersomes display elongated motion trajectories compared to their spherical counterparts. (c) MSD profiles comparison of cucurbit and spherical polymersomes. Reproduced with permission from (ref. 146). Copyright 2021 America Chemical Society.

polymersomes, allowing for the creation of enzyme-powered nanomotors. This method allowed for precise control over the amount of enzyme incorporated and the maintenance of structure during the process. The cucurbit-shaped AIE-nanomotors demonstrated significantly better motility compared to spherical AIE-nanomotors when fuelled by naturally occurring substrates (urea), achieving higher diffusion coefficients and mean squared displacement (MSD) compared with spherical polymersomes. The cucurbit AIE-polymersomes showed high biocompatibility with human cervical cancer cells (HeLa cells) in MTT assays, indicating their potential for use in healthcare applications. The successfully engineered cucurbit-shaped AIE-polymersomes with enhanced motility and functionality through enzyme integration methods, open new avenues for therapeutic applications in biomedicine. By integrating functionalities like AIE, polymersome nanomotors can provide not only precise therapeutic delivery but also real-time imaging of their journey and interaction with cells, assisting in the diagnosis and monitoring of treatment outcomes.[149,151,152]

Dynamic motion control and regulation

Polymersome-based nanomotors can be propelled *via* several mechanisms including chemical reactions, external fields (magnetic or electrically responsive), or environmental changes.[79,153] For instance, the decomposition of hydrogen peroxide by platinum nanoparticles generates oxygen bubbles, which provide thrust for polymersome propulsion.[154] Endogenous fuels, such as glucose and urease, can also be used in conjunction with enzyme-based catalysts, allowing polymersome nanomotors to operate in more biologically compatible environments.[127,146] The propulsion behaviors can be tuned by controlling the fuel concentration, catalyst density, and polymersome surface properties, ensuring efficient movement through biological fluids. However, dynamic control of the motion of polymersome-based nanomotors is challenging, which is essential for optimizing their performance in various applications.[155] Motion regulation of nanomotors in a precisely controlled manner enables tuning their activity in both time and space.[156] This is critical in biomedical applications such as targeted drug delivery, where nanomotors can remain inactive (off) while traveling through non-target regions, and be activated (on) only at the specific site of interest.[157] This selective activation allows drug release at the desired location and efficiently improves the therapeutic interventions while minimizing side effects.[158] This triggered activation enables precisely-controlled and localized therapy, which is particularly useful in treating diseases that have a specific microenvironment such as cancers, inflammatory diseases, and infections. In addition, dynamic control in the "on–off" state also allows nanomotors to operate only when necessary, conserving energy, while preventing unnecessary motion and interaction with other cells or materials.[157] This enhances the overall efficiency of nanomotors by ensuring that they are only active during key operational stages, such as delivering cargo or performing a specific therapeutic function. The ability to dynamically control the on–off motion of nanomotors, triggered by external or internal stimuli, adds a significant level of precision, efficiency, and safety to their design.[159] This innovation holds great promise for targeted therapies, energy-efficient systems, and adaptive nanotechnology applications.

Polymersome nanomotors can be engineered to switch their motion between "on" and "off" states in response to environmental stimuli, such as changes in temperature or specific biomolecules.[77,78,154] These stimuli-responsive systems can modulate the speed, direction, or mode of propulsion, allowing polymersome nanomotors to navigate and operate effectively in

complex biological environments, adding a layer of specificity and functionality to their operation. Engineering polymersome nanomotors with dynamic control introduces a level of adaptability and programmability, which offer exciting opportunities across various scientific and technological fields. This is key for creating smart, autonomous systems capable of carrying out multiple stages of operation in complex environments like the human body. Several appealing strategies have been proposed to endow polymersome nanomotors with dynamic regulation. For instance, Tu *et al.* demonstrated a nanomotor system that integrates a thermally responsive regulatory mechanism to control movement through the use of a stimuli-responsive valve or brake (Fig. 10a).[77] Polymeric stomatocytes from PEG-*b*-PS block copolymers with entrapped platinum nanoparticles (PtNPs) were used as nanomotors. They introduced temperature-responsive poly(*N*-isopropyl acrylamide) (PNIPAM) brushes onto the surface of the nanomotors using surface-initiated atom-transfer radical polymerization. The PNIPAM brushes exhibited lower critical solution temperature (LCST) behavior, collapsing at temperatures above their LCST to form a hydrophobic layer that restricts fuel access. The functioning of the thermally responsive valve was demonstrated by tracking the movement of the nanomotors at varying temperatures (30 °C and 40 °C). Below the LCST, the PNIPAM brushes were swollen, allowing hydrogen peroxide fuel to enter the motor, enabling propulsion. Conversely, when the temperature exceeded the LCST, the brushes collapsed, halting movement due to restricted fuel access. The introduction of a temperature-responsive mechanism allows for efficient and reversible control of the nanomotor's speed without altering its shape or catalytic activity. This strategy can be utilized to regulate the speed of such nanomotors dynamically, which would enhance their utility in applications like targeted drug delivery and responsive nanotechnology.

The transient behavior of motors observed in living organisms is characterized by competing activation and deactivation processes. This can be replicated in synthetic motor systems for the regulation of propulsion in nanomotors depending on the input of biomolecules and their consumption.[160,161] For instance, inspired by the dynamic and adaptive behaviors observed in natural systems, Che *et al.* used adenosine triphosphate (ATP) as a mediator for controlling transient

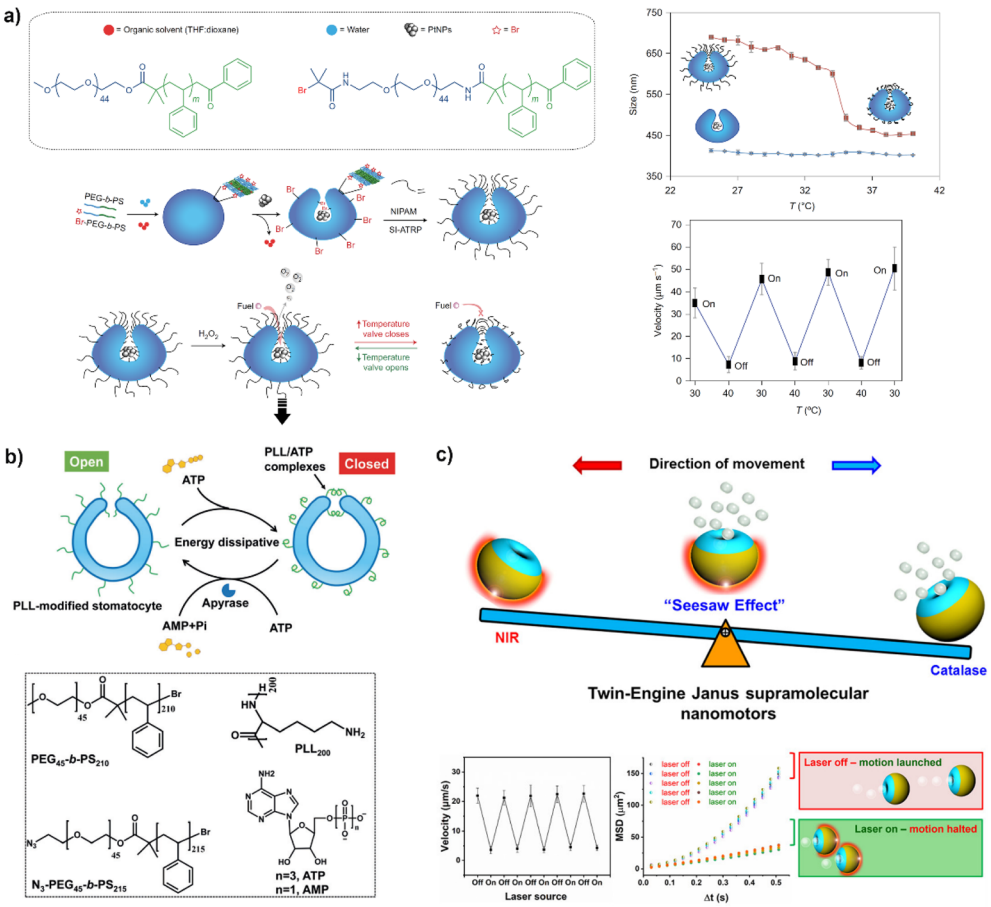

Fig. 10 (a) A self-propelled nanomotor system that integrates a thermally responsive regulatory mechanism to control movement through the use of a stimulus-responsive valve. Reproduced with permission from (ref. 77). Copyright 2017 Springer Nature. (b) ATP acts as a mediator for controlling transient behaviors in synthetic stomatocyte nanomotors composed of PEG-*b*-PS block copolymers loaded with platinum nanoparticles. Reproduced with permission from (ref. 154). Copyright 2019 Wiley. (c) Twin-engine Janus supramolecular nanomotors that leverage two distinct propulsion mechanisms including enzyme-powered motion and photothermal-activated motion. Reproduced with permission from (ref. 162). Copyright 2022 America Chemical Society.

behaviors in synthetic stomatocyte nanomotors composed of PEG-*b*-PS block copolymers loaded with platinum nanoparticles (Fig. 10b).[154] The surface of these nanomotors was modified with polylysine (PLL) to enable dynamic complexation with ATP, resembling biological mechanisms of activation and deactivation mediated by enzyme interactions. The combination of ATP and apyrase was employed to switch the motility of the nanomotors on and off, showcasing the ability to achieve controlled movement through transient binding and unbinding events. The interactions between ATP and PLL were exploited to achieve transient changes in the size of the stomatocyte openings through a hydrophobic collapse mechanism. The binding of ATP induced a collapse of PLL, which narrowed the stomatocyte opening and restricted substrate entry, effectively controlling motion activity. The decomposition of ATP by apyrase allowed for a reversal of the closed state of the stomatocyte, enabling substrate diffusion and restoring motion activity. In addition, horseradish peroxidase (HRP) was also encapsulated within the stomatocytes to form stomatocyte nanoreactors, in which the activity of HRP (oxidation of a substrate (3,3′-dimethoxybenzidine)) was influenced *via* varying concentrations of ATP and apyrase. The work presents a significant step towards creating synthetic systems that exhibit out-of-equilibrium behavior similar to that seen in living organisms. By incorporating mechanisms of ATP-mediated transient behavior, this approach opens pathways for future applications in synthetic biology and nanotechnology.

Traditional single-mode nanomotors usually face challenges in fuel availability, limiting their functionality in certain environments, and the precise control of their motion. The need for more robust and versatile propulsion systems that can operate under varied conditions motivated the design and development of dual-mode nanomotors.[159] Shao *et al.* recently explored an emerging class of twin-engine Janus supramolecular nanomotors that leverage two distinct propulsion mechanisms including enzyme-powered motion and photothermal-activated motion (Fig. 10c).[162] They first synthesized spherical polymersomes from the amphiphilic PEG-*b*-PS block copolymer. Then a hemispherical gold layer was applied to one side of the polymersomes using a sputter coating technique, allowing the particles to respond to NIR light for propulsion. Next, Janus stomatocytes were created through an osmotic shock-induced shape change process, which led to the indentation of the non-coated side of the particles. Catalase was encapsulated during this transformation, acting as the enzymatic engine for propelling motion. The stomatocyte nanomotors displayed three types of movement including photothermal propulsion (*via* the Au coating), enzyme-driven propulsion (*via* encapsulated catalase), and combination propulsion (integrating two engines). *Via* adjusting specific laser powers and fuel concentration, a motion based on both stimuli was demonstrated. By utilizing both mechanisms in conjunction, the concept of counterbalanced motion—a "seesaw effect"—was attained, where the two propulsion modes interfered with each other's motion, enabling controllable behavior. The successful combination of chemical and light-induced propulsion in a single nanomotor allows for enhanced control over motility and directionality under varying conditions. The findings indicate potential applications in complex tasks like cellular transport, environmental clean-up, and therapeutic delivery systems, thereby extending the practical usage of nanomotors in real-world scenarios.

Biomedical applications of polymersome nanomotors

Engineering nanomotors *via* adapting biological concepts and biomimicry design enables them to optimize their performance in biomedical applications.[86,163] For instance, sperm-inspired nanomotors, mimicking the flagellar motion of spermatozoa, exhibited efficient propulsion in complex environments like reproductive tracts or tissues.[164] These designs offer high motility and adaptability, making them ideal for applications like assisted reproduction or targeting hard-to-reach sites in the body. Nanomotors with small sizes, controllable and active movement, and the ability to navigate complex biological environments such as blood, mucus, or tissue, open up opportunities for applications that traditional medical technologies cannot achieve.[165] Their active propulsion allows them to swim in bodily fluids, where they can capture and neutralize toxins or pathogens, enhancing the efficacy of real-time diagnostics and biosensing.[166,167] A key advantage of nanomotors is their ability to precisely regulate speed and directionality, ensuring that therapeutic payloads reach specific sites under optimal conditions.[168,169] This precision significantly improves the accuracy of drug delivery and therapeutic actions, minimizing off-target effects and reducing damage to healthy tissues. Nanomotors can be guided by external controls (such as magnetic or light fields) in real-time or directed by gradients in biological environments (such as pH or chemical concentration), providing control over their path, speed, and timing of the therapeutic release.[49,170] In addition, nature-inspired surface modifications further enhance the functionality of nanomotors by improving biocompatibility, reducing immune recognition, and extending circulation times.[171,172] For instance, by mimicking the properties of red blood cells—optimized for navigating blood vessels and avoiding immune detection—micro/nano-motors can be designed to prolong their activity within the body.[173] Additionally, by emulating the collective behavior of organisms like fish or ants, nanomotors can be programmed to self-organize and operate in swarms. Swarm behavior is a fundamental characteristic of nanomotors, enabling collective motion and enhanced functionalities beyond individual propulsion.[36,174] Inspired by natural microswimmers such as bacteria, the coordinated movement of nanomotors arises from interactions among individual units and external stimuli, such as chemical gradients, magnetic fields, or light irradiation.[175–177] This collective behavior enabled them to perform complex tasks such as enhancing cargo transport efficiency, increasing targeting precision, and facilitating the penetration of biological barriers.[175,176,178] This collective action boosts their potential for improving therapeutic outcomes and diagnostic precision.

Polymersome-based nanomotors offer significant potential due to their versatility, and tunable structural features, which can be harnessed for bio-related applications such as targeted drug delivery, controlled release, diagnostics, and environmental remediation.[24,179] The chemical flexibility of polymersomes allows for functionalization with targeting ligands (such as peptides, antibodies, or aptamers) to enhance selective binding to specific cells or tissues.[70] This improves the targeting efficiency of drug delivery systems and reduces off-target effects. By adjusting the hydrophobic and hydrophilic blocks, polymersomes can be fine-tuned with key parameters such as size, morphology, stability, and permeability, optimizing them for drug loading and controlled release.[24] The use of stimuli-responsive polymers (such as pH-sensitive, temperature-sensitive, or redox-sensitive materials) allows polymersome nanomotors to release their therapeutic cargo in response to specific environmental cues.[48,76] For example, pH-sensitive polymers can respond to the acidic environment of tumor tissues, triggering drug release precisely at the target site. In addition, polymersome nanomotors employing inherently asymmetric shapes have also shown potential advantages due to the crucial influence of shape on factors such as propulsion efficiency, cellular uptake and biodistribution.[180,181] By engineering different shapes (*e.g.*, spherical, rod-like, or stomatocyte structures), polymersome nanomotors can achieve optimized propulsion. For instance, rod-shaped nanomotors have been shown to exhibit more efficient propulsion in viscous biological fluids compared to spherical ones, making them ideal for navigating complex environments such as blood or mucus.[182,183] The shape of nanomotors also influences their interaction with biological systems. Rod-shaped or elongated delivery systems have demonstrated prolonged circulation times due to geometry factors, and enhanced cellular uptake due to their increased contact surface area with cell membranes, leading to more efficient drug delivery.[184,185] Additionally, elongated shapes can penetrate deeper into tissues, improving the distribution of therapeutic agents in dense tumor environments.[186] Thus, the inherent asymmetrical shape of polymersome nanomotors offers significant advantages, making them highly suitable for targeted drug delivery and other therapeutic applications.

Enhanced delivery

Chemical–physical properties of nanoparticles including the size, shape, and surface charge are determining factors that influence their behavior and final fate in biomedical applications.[15,187,188] For nanomotors, size control at the nanoscale is a significant parameter because the physical dimensions of these devices significantly influence their behaviors and properties such as circulation time, cellular uptake, biodistribution, and the ability to overcome biological barriers.[189] For example, nanomotors with a size of 20–200 nm are typically optimal for

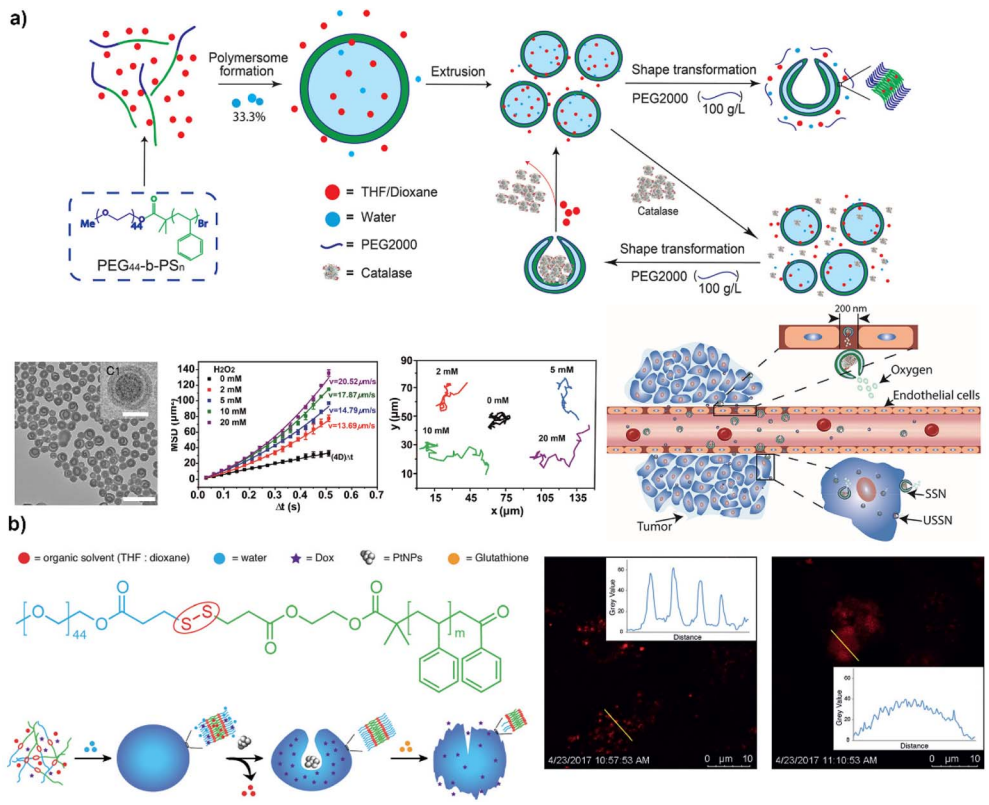

Fig. 11 (a) Enzyme-powered ultra-small polymersome nanomotors with controllable size for biomedical applications. Reproduced with permission from (ref. 85). Copyright 2019 America Chemical Society. (b) A redox-sensitive stomatocyte nanomotor system for triggered drug release. Reproduced with permission from (ref. 75). Copyright 2017 Wiley.

cellular uptake through endocytosis, while smaller or larger particles may be less efficiently internalized. Proper size control ensures nanomotors can efficiently enter cells and deliver their cargo. Larger nanomotors (above 200 nm) are more likely to be recognized and engulfed by immune cells (such as macrophages), leading to rapid clearance from the body. Smaller nanomotors, on the other hand, can evade immune detection more effectively, allowing for longer circulation time. However, usually, polymersome nanomotors display a size >300 nm, which is not favorable for the endocytosis process and circulation in the blood. To cope with such an issue, Sun *et al.*, presented enzyme-powered polymersome nanomotors with controllable size for biomedical applications (Fig. 11a).[75] Extrusion techniques were utilized to achieve uniform, ultrasmall polymersomes (from PEG-PS) as a precursor for the nanomotor fabrication. The addition of a trace amount of polyethylene glycol (PEG) was then applied to induce the shape transformation of the ultrasmall polymersomes (around 150 nm) into stomatocyte structures, significantly smaller than previously reported nanomotors. Catalase was encapsulated within the stomatocyte cavity during the shape transformation process, which can propel the nanomotor *via* the decomposition of hydrogen peroxide (H_2O_2, 2 mM) into oxygen. This approach preserved enzyme activity significantly better than previous methods such as the dialysis approach to remove organic solvents. The smaller size of nanomotors (compared to previously developed nanomotors) facilitates enhanced penetration across biological barriers. This includes better passage through the vasculature (demonstrated using a pulmonary artery endothelial cell model) and increased ability to reach tumor tissues *via* the enhanced permeation and retention (EPR) effect. The increased penetration was observed both with and without the addition of fuel (H_2O_2), indicating that the size alone is a major factor. The smaller size also led to improved cellular uptake. Experiments with HeLa cells showed significantly higher internalization of smaller-sized nanomotors compared to larger stomatocyte nanomotors both with and without the addition of fuel. The increased uptake was attributed to both the smaller size and the active motion of the motors, making them promising candidates for various biomedical applications.

Controlled release

Polymersome nanomotors are usually constructed from PEG-PS-based self-assemblies, which display a facile ability to undergo morphology transformation for catalyst entrapment.[92] However, the non-degradable properties of polystyrene-based blocks hinder cargo release capacity, which limits their utility in biomedical-related fields. Polymer blending for controlled self-assembly is a powerful strategy in materials science, especially for developing functional nanomaterials with precise structures and tailored properties.[128] By combining polymers with complementary properties, the morphology, phase behavior, and kinetics of self-assemblies can be fine-tuned, enabling the formation of complex and hierarchical structures. This approach offers a versatile pathway for developing advanced, responsive, and biocompatible materials for biomedical and industrial use. Tu *et al.* presented the fabrication of a biodegradable hybrid stomatocyte nanomotor for drug delivery and controlled release.[125] The stomatocyte structure was formed by blending poly(ethylene glycol) (PEG)-*b*-poly(ε-caprolactone) (PCL) (biodegradable) and PEG-*b*-PS (well-established vesicle former). The different properties of PCL (semicrystalline) and PS (glassy) were leveraged to create PCL domains within the stomatocyte membrane. This combination provided both biodegradability and the structural integrity necessary for stomatocyte formation and drug encapsulation, even at high PCL percentages (up to 50%). Controlled demixing led to pore formation upon PCL degradation, enabling sustained and controlled drug release. The drug release was further modulated by the local pH, accelerating release in acidic environments mimicking the tumor microenvironment. The incorporation of platinum nanoparticles (PtNPs) provided the catalytic activity needed to convert hydrogen peroxide into motion. The combination of self-propulsion and pH-sensitive drug release allows for targeted drug delivery. Upon reaching the target, the acidic environment within the tumor cells promotes drug release, potentially enhancing therapeutic efficacy. The versatility of polymer chemistry also enables the incorporation of stimuli-responsiveness with polymersome nanomotors, which is of critical value for the controlled release in biomedical applications.[190,191] Tu *et al.* presented a redox-sensitive stomatocyte nanomotor system for triggered drug release (Fig. 11b).[76] They synthesized a redox-sensitive block copolymer PEG-SS-PS functionalized with a disulfide linkage *via* atom transfer radical polymerization (ATRP) using a PEG-SS-Br macroinitiator. Polymersomes were formed by a solvent switch method, and doxorubicin was encapsulated during the self-assembly process. An osmotic shock during dialysis induced the morphology change to stomatocytes, trapping the platinum nanoparticles in the cavities. The incorporation of a disulfide bridge between the hydrophilic PEG and hydrophobic PS blocks of the block copolymer rendered the nanomotor sensitive to reducing agents like glutathione (GSH), a molecule abundant intracellularly but less so extracellularly. Upon enhanced delivery, the presence of intracellular GSH cleaved the disulfide bond, causing the PEG shell to detach, leading to aggregation, cessation of movement, and drug release. The nanomotor is multifunctional, combining self-propulsion (*via* decomposition of H_2O_2), environmental sensing (*via* the redox-sensitive disulfide bond), and drug delivery (*via* doxorubicin loaded into the lumen).

Deeper tissue penetration

Polymersome nanomotors are promising candidates for overcoming biological barriers due to their active propulsion, enabling them to move autonomously through complex biological fluids and tissues, providing advantages over passive diffusion.[136] These delivery vehicles with active motility represent a novel frontier in nanomedicine, particularly for applications that require deep tissue penetration, such as drug delivery, tumor treatment, and regenerative medicine. In cancer

therapy, nanomotors in the range of 50–150 nm are the most effective at penetrating and accumulating in tumors, as they are small enough to pass through the gaps in tumor vasculature but large enough to be retained in the tumor environment without being cleared too quickly.[181,192] Smaller nanomotors can penetrate deeper into tumor tissues, whereas larger ones may be confined to the periphery. Size control allows for tuning the penetration depth, which is critical for delivering drugs to the interior of dense tumors. To showcase such utility of polymersome nanomotors, Shao *et al.* presented an alternative strategy to drug delivery and tissue penetration using photoactivated polymersome nanomotors (Fig. 12a).[48] The concept lies in the creation of nanoscale (*ca.* 100 nm) motors, which are crucial for traversing biological barriers for intracellular cargo delivery and deep tissue penetration, addressing limitations of existing micro-scale motors and passive delivery methods. These polymersome nanomotors utilized biodegradable poly(ethylene glycol)-*b*-poly(D, L-lactide) (PEG-PDLLA) block copolymers linked by a pH-sensitive imine bond. This ensured biocompatibility and avoided the accumulation of non-degradable materials. The asymmetric design—a hemispherical gold nanocoating on a polymersome—created a Janus morphology, critical for directional movement in response to the thermal gradient generated by NIR irradiation. The use of NIR irradiation for activation both allowed a more effective penetration of biological tissues and remote control and targeted drug delivery. The polymersome nanomotors demonstrated the capacity for both intracellular delivery of internal cargo and facilitated transport of external agents to the cell, expanding the therapeutic potential. Upon intracellular delivery, an acidic environment in the endosome led to the release of cargoes encapsulated in the polymersome nanomotors. In addition, upon NIR irradiation, the ~100 nm polymersome nanomotors exhibited a significantly enhanced penetration effect into 3D HeLa tumor spheroids compared to the control polymersomes. This demonstrated that the motility conferred by the gold coating and NIR activation significantly improved the ability of the nanomotors to traverse the complex 3D tumor environment.

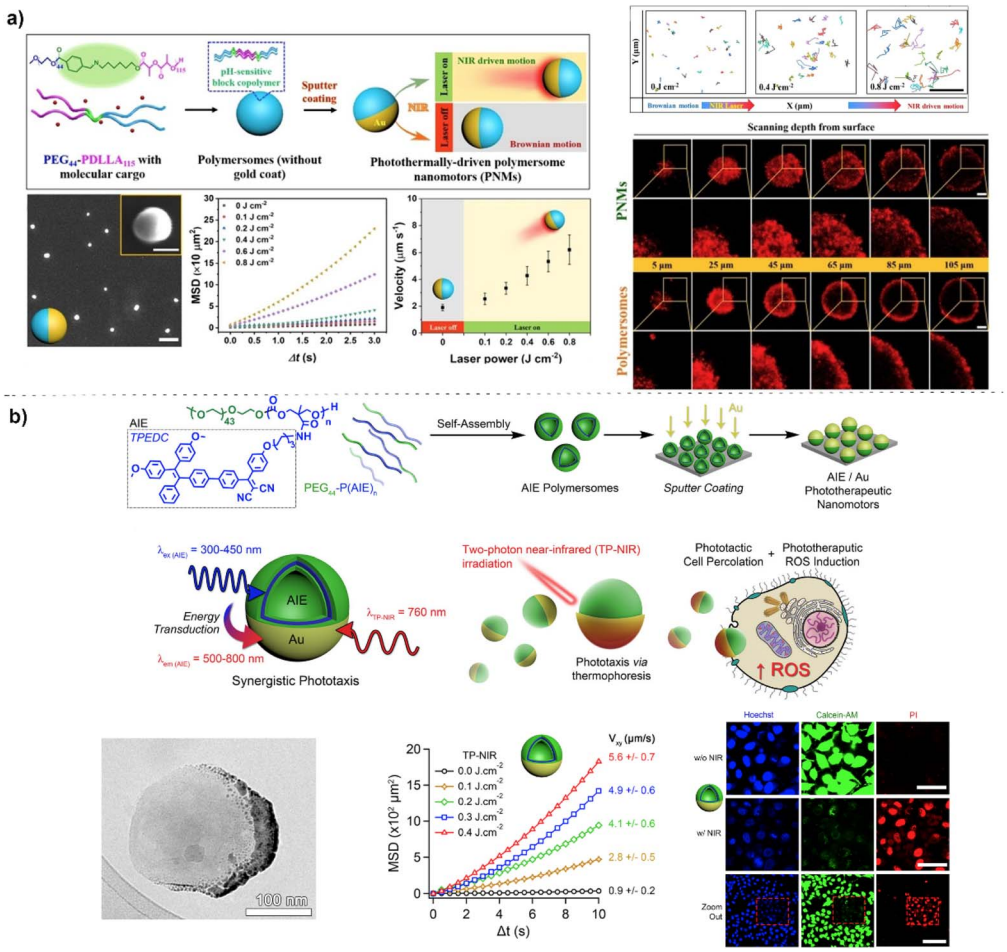

Fig. 12 (a) Photoactivated polymersome nanomotors towards enhanced drug delivery and tissue penetration. The nanomotors are prepared from PEG-PDLLA polymersomes *via* a sputter coating approach, which displayed motility upon NIR light irradiation. This motility facilitated enhanced penetration into 3D HeLa tumor spheroids. Reproduced with permission from (ref. 48). Copyright 2022 Wiley. (b) Photoactivated nanomotors displayed theranostic applications from polymersomes incorporated with AIE moieties. The polymersome nanomotors combined AIE imaging, photo-active motility, PDT, and PTT in a single nanomotor platform. Reproduced with permission from (ref. 201). Copyright 2021 Springer Nature.

Further, polymersome nanomotors showed significant toxicity to the cancer cells after NIR irradiation in the 3D spheroids, demonstrating a potential therapeutic effect. The combination of several innovative design features including biodegradability, nanoscale dimensions, NIR activation, controlled release, and active motility in a single nanomotor system for targeted drug delivery and deeper tissue penetration represents a significant advancement in nanomotor technology.

Biomedical theranostics

Nanomotors can also be designed as theranostic platforms with motility, integrating both therapeutic and diagnostic functions, which is a rapidly advancing field in biomedical research.[70,193] This is usually realized *via* carrying drugs or therapeutic agents while simultaneously providing imaging function *via* fluorescent or photoacoustic agents.[69] Nanomotors can be modified with light-responsive materials or photosensitizers (*e.g.*, chlorin e6 for photodynamic therapy), offering controlled delivery and activation of therapy *in situ*.[194,195] This dual function enables healthcare providers to track the localization of nanomotors, monitor therapeutic effects, and adjust treatment regimens based on real-time feedback on the therapeutic process. Polymersome nanomotors are particularly suited for theranostic applications due to their unique combination of active propulsion, multifunctional capabilities, and tunable polymer-based structures. Conventional polymersome-based theranostic platforms usually suffer from several issues such as burst release, aggregation-induced quenching, and photobleaching. An alternative choice is to functionalize polymersomes with aggregation-induced emission (AIE) moieties.[152,196–198] AIE molecules are ideal for theranostic applications because they remain "off" in the dispersed state and emit strong fluorescence when aggregated.[199] This property can help track nanomotor movement and accumulation in target tissues, enabling both diagnostic imaging and photo-therapy (PDT and PTT) for cancer treatment.[200] Cao *et al.* presented photoactivated nanomotors for enhanced phototherapy (PDT) (Fig. 12b).[201] They synthesized well-defined amphiphilic poly(ethylene glycol) (PEG)-poly(trimethylene carbonate) (PTMC) copolymers with a high density (>60 wt%) of a second-generation AIE molecule (PEG-PAIE).[202] The copolymer's design facilitated self-assembly into polymersomes with controlled size and morphology (300–500 nm). A hemispherical gold nanoshell was deposited onto one side of the pre-formed AIE polymersomes using a turbo sputter coater, which created the asymmetric structure necessary for the thermophoretic propulsion mechanism. Cryo-TEM and cryo-electron tomography were employed to verify the integrity of the polymersome structure after gold coating. The core innovation lies in the synergistic combination of aggregation-induced emission (AIE) and plasmonic gold nanoshells within a single biodegradable polymersome nanomotor. Biodegradable block copolymers decorated with AIE motifs generated reactive oxygen species (ROS) upon two-photon near-infrared (TP-NIR) irradiation, providing the phototherapeutic element. Asymmetric Au nanoshells acted as an energy sink for AIE fluorescence, converting radiant energy into heat to drive

Table 1 Representative engineering strategy, mechanisms of active motion and biomedical applications of polymersome-based nanomotors are summarized in the table

Polymeric materials	Fabrication strategy	Catalytic engine	Mechanism of active motion	Biomedical applications	Ref.
PEG-PDLLA	Sputter coating metal species on the half side of polymersomes	Au nanoparticles	Thermophoresis motion *via* light irradiation	Controlled release	48
PEG-PS	Sputter coating metal species on the half side of polymersomes	Pt nanoparticles	O_2 bubble-induced motion *via* H_2O_2 decomposition	Deeper penetration across vasculature model	67
PEG-PS	Encapsulation of catalytic species inside polymersome stomatocytes	Pt nanoparticles	O_2 bubble-induced motion *via* H_2O_2 decomposition	Enhanced delivery of molecular drug	75 and 92
PEG-PDLLA	Conjugation of enzyme on the surface of polymeric nanotubes	Catalase	O_2 bubble-induced motion *via* H_2O_2 decomposition	—	126
PEG-PDLLA	Spatial conjugation of catalytic species in polymersome stomatocytes	GOX and HRP	O_2 bubble-induced motion *via* cascade reaction	—	127
PMPC-PDPA/POEGMA-PDPA	Encapsulation of enzymes in asymmetrical polymersomes	GOX and/or HRP	Substrate gradient-induced chemotactic motion	Enhanced crossing blood–brain barrier	128
PEG-PDLLA	*In situ* formation of catalytic species inside polymersome stomatocytes	MnO_2 nanoparticle	O_2 bubble-induced motion *via* H_2O_2 decomposition	Rescue cells from ROS stress	141
PEG-PDLLA	*In situ* formation of metal shell around polymersome stomatocytes	Au nanoshell	Thermophoresis motion *via* light irradiation	Enhanced delivery of siRNA	145
PEG-PAIE	Trap catalytic enzymes on the surface of asymmetrical polymersomes *via* LBL	Urease	Self-diffusiophoresis motion *via* urea hydrolysis	—	146
PEG-PAIE	Sputter coating metal species on the half side of polymersomes	Au nanoparticles	Thermophoresis motion *via* light irradiation	Imaging and photodynamic therapy	201

thermophoretic motility, leading to enhanced directional movement compared to controls lacking AIE units. The nanomotor exhibited both phototaxis (directed movement in response to light) and phototherapeutic capabilities, all driven by a single TP-NIR stimulus. *In vitro* studies confirmed enhanced cellular uptake, ROS production, and apoptosis upon TP-NIR activation, achieving highly localized and efficient cell killing. These results highlight the potential of this technology for precise and effective cancer treatment, which represents a significant advancement in both nanomotor design and targeted phototherapy.

Conclusions

Polymersome-based nanomotors have shown significant promise in biomedical applications, particularly in drug delivery, diagnostics, and precision therapy. The unique structural properties of polymersomes, such as their hollow vesicle-like morphology, biocompatibility, tunable size, and ability to encapsulate hydrophilic and hydrophobic agents, make them ideal candidates for use in the design and construction of active delivery systems. Polymersome nanomotors displaying active propulsion mechanisms—powered by chemical, enzymatic, or external stimuli, are summarized in Table 1. Polymersome nanomotors have demonstrated a wide range of biomedical utilities including enhanced tissue penetration, precise cargo delivery, responsiveness to biological stimuli, and multi-mode theranostic treatment, giving them a critical edge over traditional passive delivery systems. The development of polymersomes with tailored physical–chemical properties, coupled with self-propelled motility, paves the way for smarter and more efficient delivery platforms capable of overcoming biological barriers and increasing therapeutic precision.

While the field has witnessed considerable progress in the fabrication, motion control, and application of polymersome-based nanomotors, considerable challenges still remain. For instance, current propulsion mechanisms of polymersome nanomotors often rely on fuel sources like hydrogen peroxide, which can be toxic in biological systems. There is a need to develop propulsion systems that operate efficiently in physiological conditions, utilizing biofriendly fuels or external stimuli for safe *in vivo* applications. Additionally, controlling the precise movement and behavior of nanomotors in complex, dynamic biological environments are still difficult, with limited control over their interactions with immune cells, off-target accumulation, and clearance from the body. Future designs of polymersome nanomotors are expected to incorporate more sophisticated control mechanisms, allowing nanomotors to respond dynamically to environmental stimuli such as pH, temperature, or specific biomolecular signals. This may allow them to change shape, surface properties, or propulsion mechanisms in response to environmental signals similar to how biological organisms adapt to their surroundings, thus improving the adaptability of polymersome nanomotors in complex biological environments. Improvements in navigation through biological fluids, immune evasion, and prolonged circulation time are crucial. Additionally, nanomotors that combine diagnostics, imaging, and therapy (theranostics) will become increasingly important in engineering multi-functional polymersome nanomotors.

While polymersome nanomotors mainly found utilities at cellular level, their *in vivo* stability and degradation are key concerns for biomedical applications. Surface modifications like PEGylation can prolong circulation time, but protein adsorption, enzymatic degradation, and pH sensitivity affect functional lifespan. While degradation products of polymeric materials are generally biocompatible, risks such as immune clearance *via* the reticuloendothelial system (RES) and unintended inflammatory responses must be addressed. Future research should focus on biodegradable, stimuli-responsive polymers to enhance safety and adaptability, which is critical to facilitate clinical translation. In addition, leveraging biomaterials and biomimetic designs, the development of biodegradable nanomotors that degrade into harmless byproducts in the body will be helpful for reducing potential long-term toxicity or accumulation issues. The advanced polymersome nanomotors may incorporate more complex biomimetic interfaces that enable them to interact seamlessly with biological tissues, possibly incorporating natural cell membranes or biomolecule-coated surfaces that mimic the body's structures to avoid immune detection. Advanced surface modifications, such as ligands or antibodies, should also be explored to enhance specific targeting of diseased tissues.

Addressing challenges in large-scale, cost-effective fabrication and ensuring regulatory compliance will be critical for transitioning polymersome nanomotors from laboratory research to clinical applications. In addition, regulatory barriers and safety concerns are critical factors in the clinical translation of polymersome nanomotors. Unlike traditional passive nanocarriers, the dynamic nature of nanomotors introduces additional complexities in assessing biodistribution, clearance mechanisms, and potential off-target effects. Standardized protocols for large-scale production, quality control, and reproducibility must also be established to meet regulatory approval. Addressing these challenges through rigorous preclinical studies and early engagement with regulatory agencies will be essential for advancing polymersome nanomotors toward future clinical applications.

Data availability

No primary research results, software or code have been included and no new data were generated or analysed as part of this review.

Author contributions

All authors contributed to the writing and revision of the Manuscript.

Conflicts of interest

The authors declare no competing financial interest.

Acknowledgements

This work was supported by the National Natural Science Foundation of China (12302410, 52403198), the Sichuan Science and Technology Program (2024YFHZ0356), and the Fundamental Research Funds for the Central Universities.

References

1 B. C. Buddingh' and J. C. M. van Hest, *Acc. Chem. Res.*, 2017, **50**, 769–777.
2 Y. Tu, F. Peng, A. Adawy, Y. Men, L. K. E. A. Abdelmohsen and D. A. Wilson, *Chem. Rev.*, 2016, **116**, 2023–2078.
3 S. Song, T. Ivanov, T. P. Doan-Nguyen, L. C. da Silva, J. Xie, K. Landfester and S. Cao, *Angew. Chem., Int. Ed.*, 2025, **64**, e202418431.
4 S. Song, T. Ivanov, D. Yuan, J. Wang, L. C. da Silva, J. Xie and S. Cao, *Biomacromolecules*, 2024, **25**, 5468–5488.
5 S. E. Sherman, Q. Xiao and V. Percec, *Chem. Rev.*, 2017, **117**, 6538–6631.
6 S. Cao, T. Ivanov, J. Heuer, C. T. J. Ferguson, K. Landfester and L. Caire da Silva, *Nat. Commun.*, 2024, **15**, 39.
7 S. Cao, P. Zhou, G. Shen, T. Ivanov, X. Yan, K. Landfester and L. Caire da Silva, *Nat. Commun.*, 2025, **16**, 2407.
8 T. Ivanov, T. P. Doan-Nguyen, M. A. Belahouane, Z. Dai, S. Cao, K. Landfester and L. Caire da Silva, *Macromol. Rapid Commun.*, 2024, **45**, 2400626.
9 A. Rösler, G. W. M. Vandermeulen and H.-A. Klok, *Adv. Drug Delivery Rev.*, 2001, **53**, 95–108.
10 H. Liu, H.-H. Lu, Y. Alp, R. Wu and S. Thayumanavan, *Prog. Polym. Sci.*, 2024, **148**, 101765.
11 J. Jennings, G. He, S. M. Howdle and P. B. Zetterlund, *Chem. Soc. Rev.*, 2016, **45**, 5055–5084.
12 G. K. K. Clothier, T. R. Guimarães, S. W. Thompson, J. Y. Rho, S. Perrier, G. Moad and P. B. Zetterlund, *Chem. Soc. Rev.*, 2023, **52**, 3438–3469.
13 S. Varlas, S. B. Lawrenson, L. A. Arkinstall, R. K. O'Reilly and J. C. Foster, *Prog. Polym. Sci.*, 2020, **107**, 101278.
14 J. Wan, B. Fan and S. H. Thang, *Chem. Sci.*, 2022, **13**, 4192–4224.
15 H. Cabral, K. Miyata, K. Osada and K. Kataoka, *Chem. Rev.*, 2018, **118**, 6844–6892.
16 X. Yang, Y. Chen, M. Wang, H. Zhang, X. Li and H. Zhang, *Adv. Funct. Mater.*, 2016, **26**, 8427–8434.
17 A. Hanisch, A. H. Gröschel, M. Förtsch, M. Drechsler, H. Jinnai, T. M. Ruhland, F. H. Schacher and A. H. E. Müller, *ACS Nano*, 2013, **7**, 4030–4041.
18 J. C. M. van Hest, D. A. P. Delnoye, M. W. P. L. Baars, M. H. P. van Genderen and E. W. Meijer, *Science*, 1995, **268**, 1592–1595.
19 C. G. Palivan, R. Goers, A. Najer, X. Zhang, A. Car and W. Meier, *Chem. Soc. Rev.*, 2016, **45**, 377–411.
20 B. M. Discher, Y.-Y. Won, D. S. Ege, J. C.-M. Lee, F. S. Bates, D. E. Discher and D. A. Hammer, *Science*, 1999, **284**, 1143–1146.
21 L. M. P. E. van Oppen, L. K. E. A. Abdelmohsen, S. E. van Emst-de Vries, P. L. W. Welzen, D. A. Wilson, J. A. M. Smeitink, W. J. H. Koopman, R. Brock, P. H. G. M. Willems, D. S. Williams and J. C. M. van Hest, *ACS Cent. Sci.*, 2018, **4**, 917–928.
22 R. J. R. W. Peters, M. Marguet, S. Marais, M. W. Fraaije, J. C. M. van Hest and S. Lecommandoux, *Angew. Chem., Int. Ed.*, 2014, **53**, 146–150.
23 E. Rideau, R. Dimova, P. Schwille, F. R. Wurm and K. Landfester, *Chem. Soc. Rev.*, 2018, **47**, 8572–8610.
24 F. Wang, J. Xiao, S. Chen, H. Sun, B. Yang, J. Jiang, X. Zhou and J. Du, *Adv. Mater.*, 2018, **30**, 1705674.
25 Q. Sun, J. Shi, H. Sun, Y. Zhu and J. Du, *Biomacromolecules*, 2023, **24**, 4587–4604.
26 Y. Zheng, Y. Liu, Z. Wu, C. Peng, Z. Wang, J. Yan, Y. Yan, Z. Li, C. Liu, J. Xue, H. Tan, Q. Fu and M. Ding, *Adv. Mater.*, 2023, **35**, 2210986.
27 G. Liu, J. Tan, J. Cen, G. Zhang, J. Hu and S. Liu, *Nat. Commun.*, 2022, **13**, 585.
28 Y. Zhu, F. Wang, C. Zhang and J. Du, *ACS Nano*, 2014, **8**, 6644–6654.
29 X. Wang, C. Yao, G. Zhang and S. Liu, *Nat. Commun.*, 2020, **11**, 1524.
30 X. Hu, S. Zhai, G. Liu, D. Xing, H. Liang and S. Liu, *Adv. Mater.*, 2018, **30**, 1706307.
31 F. Wang, J. Gao, J. Xiao and J. Du, *Nano Lett.*, 2018, **18**, 5562–5568.
32 Y. Duan, Y. Wang, X. Li, G. Zhang, G. Zhang and J. Hu, *Chem. Sci.*, 2020, **11**, 186–194.
33 W. X. Gu, J. N. An, H. Meng, N. Yu, Y. A. Zhong, F. H. Meng, Y. Xu, J. Cornelissen and Z. Y. Zhong, *Adv. Mater.*, 2019, **31**, 1904742.
34 M. Zheng, Q. Du, X. Wang, Y. Zhou, J. Li, X. Xia, Y. Lu, J. Yin, Y. Zou, J. B. Park and B. Shi, *Adv. Sci.*, 2021, **8**, 2102001.
35 M. Xuan, J. Shao, C. Gao, W. Wang, L. Dai and Q. He, *Angew. Chem., Int. Ed.*, 2018, **57**, 12463–12467.
36 J. Shao, M. Xuan, H. Zhang, X. Lin, Z. Wu and Q. He, *Angew. Chem., Int. Ed.*, 2017, **56**, 12935–12939.
37 A. C. Hortelão, R. Carrascosa, N. Murillo-Cremaes, T. Patiño and S. Sánchez, *ACS Nano*, 2019, **13**, 429–439.
38 M. Xuan, Z. Wu, J. Shao, L. Dai, T. Si and Q. He, *J. Am. Chem. Soc.*, 2016, **138**, 6492–6497.
39 P. L. Venugopalan, B. Esteban-Fernández de Ávila, M. Pal, A. Ghosh and J. Wang, *ACS Nano*, 2020, **14**, 9423–9439.
40 M. Pal, N. Somalwar, A. Singh, R. Bhat, S. M. Eswarappa, D. K. Saini and A. Ghosh, *Adv. Mater.*, 2018, **30**, 1800429.
41 J. Wang, Z. Xiong, J. Zheng, X. Zhan and J. Tang, *Acc. Chem. Res.*, 2018, **51**, 1957–1965.
42 C. Simó, M. Serra-Casablancas, A. C. Hortelao, V. Di Carlo, S. Guallar-Garrido, S. Plaza-García, R. M. Rabanal, P. Ramos-Cabrer, B. Yagüe, L. Aguado, L. Bardia, S. Tosi, V. Gómez-Vallejo, A. Martín, T. Patiño, E. Julián, J. Colombelli, J. Llop and S. Sánchez, *Nat. Nanotechnol.*, 2024, **19**, 554–564.
43 L. Xu, F. Mou, H. Gong, M. Luo and J. Guan, *Chem. Soc. Rev.*, 2017, **46**, 6905–6926.
44 Y. Yu, L. Liang, T. Sun, H. Lu, P. Yang, J. Li, Q. Pang, J. Zeng, P. Shi, J. Li and Y. Lu, *Adv. Healthcare Mater.*, 2024, 2400163.
45 S. Liu, D. Xu, J. Chen, N. Peng, T. Ma and F. Liang, *Nanoscale*, 2023, **15**, 12944–12953.

46 S. Zheng, Y. Wang, S. Pan, E. Ma, S. Jin, M. Jiao, W. Wang, J. Li, K. Xu and H. Wang, *Adv. Funct. Mater.*, 2021, **31**, 2100936.
47 Z. Wu, L. Chen, W. Guo, J. Wang, H. Ni, J. Liu, W. Jiang, J. Shen, C. Mao, M. Zhou and M. Wan, *Nat. Nanotechnol.*, 2024, **19**, 1375–1385.
48 J. Shao, S. Cao, D. S. Williams, L. K. E. A. Abdelmohsen and J. C. M. van Hest, *Angew. Chem., Int. Ed.*, 2020, **59**, 16918–16925.
49 V. Garcia-Gradilla, J. Orozco, S. Sattayasamitsathit, F. Soto, F. Kuralay, A. Pourazary, A. Katzenberg, W. Gao, Y. Shen and J. Wang, *ACS Nano*, 2013, **7**, 9232–9240.
50 H. Zhang, Z. Li, C. Gao, X. Fan, Y. Pang, T. Li, Z. Wu, H. Xie and Q. He, *Sci. Robot.*, 2021, **6**, eaaz9519.
51 B. Esteban-Fernández de Ávila, W. Gao, E. Karshalev, L. Zhang and J. Wang, *Acc. Chem. Res.*, 2018, **51**, 1901–1910.
52 W. Gao and J. Wang, *Nanoscale*, 2014, **6**, 10486–10494.
53 S. Sánchez, L. Soler and J. Katuri, *Angew. Chem., Int. Ed.*, 2015, **54**, 1414–1444.
54 Y. Ye, J. Luan, M. Wang, Y. Chen, D. A. Wilson, F. Peng and Y. Tu, *Chem.–Eur. J.*, 2019, **25**, 8663–8680.
55 X. Lin, Z. Wu, Y. Wu, M. Xuan and Q. He, *Adv. Mater.*, 2016, **28**, 1060–1072.
56 S. Campuzano, B. Esteban-Fernández de Ávila, P. Yáñez-Sedeño, J. M. Pingarrón and J. Wang, *Chem. Sci.*, 2017, **8**, 6750–6763.
57 Z. Luo, R. Wang, X. Deng, T. Chen, X. Ma, Y. Zhang, C. Gao and A. Wu, *Nanoscale*, 2024, **16**, 3006–3010.
58 J. Shao, M. Abdelghani, G. Shen, S. Cao, D. S. Williams and J. C. M. van Hest, *ACS Nano*, 2018, **12**, 4877–4885.
59 J. Wu, S. Balasubramanian, D. Kagan, K. M. Manesh, S. Campuzano and J. Wang, *Nat. Commun.*, 2010, **1**, 36.
60 H. Zhao, Y. Zheng, Y. Cai, T. Xu, R. Dong and X. Zhang, *Nano Today*, 2023, **52**, 101939.
61 S. Yuan, L. Yang, X. Lin and Q. He, *Nanoscale*, 2023, **15**, 12558–12566.
62 S. Wang, J. Xu, Q. Zhou, P. Geng, B. Wang, Y. Zhou, K. Liu, F. Peng and Y. Tu, *Adv. Healthcare Mater.*, 2021, **10**, 2100335.
63 Z. Liang, Y. Tu and F. Peng, *Adv. Healthcare Mater.*, 2021, **10**, 2100720.
64 J. Ou, K. Liu, J. Jiang, D. A. Wilson, L. Liu, F. Wang, S. Wang, Y. Tu and F. Peng, *Small*, 2020, **16**, 1906184.
65 I. Ortiz-Rivera, M. Mathesh and D. A. Wilson, *Acc. Chem. Res.*, 2018, **51**, 1891–1900.
66 T. Lammers, S. Aime, W. E. Hennink, G. Storm and F. Kiessling, *Acc. Chem. Res.*, 2011, **44**, 1029–1038.
67 F. Peng, Y. Men, Y. Tu, Y. Chen and D. A. Wilson, *Adv. Funct. Mater.*, 2018, **28**, 1706117.
68 J. Wang, A. Polyviou, J. F. Scheerstra, S. Cao, A. D. Fusi, J. Shao and J. C. M. van Hest, *J. Mater. Chem. B*, 2025, **13**, 2820–2825.
69 S. M. Hosseini, J. Mohammadnejad, S. Salamat, Z. Beiram Zadeh, M. Tanhaei and S. Ramakrishna, *Mater. Today Chem.*, 2023, **29**, 101400.
70 M. Beygi, F. Oroojalian, S. S. Hosseini, A. Mokhtarzadeh, P. Kesharwani and A. Sahebkar, *Prog. Mater. Sci.*, 2023, **140**, 101209.
71 C. K. Wong, M. H. Stenzel and P. Thordarson, *Chem. Soc. Rev.*, 2019, **48**, 4019–4035.
72 X. Zhang, J. C. M. van Hest and Y. Men, *ACS Appl. Nano Mater.*, 2024, **7**, 14865–14888.
73 C. K. Wong, A. D. Martin, M. Floetenmeyer, R. G. Parton, M. H. Stenzel and P. Thordarson, *Chem. Sci.*, 2019, **10**, 2725–2731.
74 H. Sun, D. Liu and J. Du, *Chem. Sci.*, 2019, **10**, 657–664.
75 J. Sun, M. Mathesh, W. Li and D. A. Wilson, *ACS Nano*, 2019, **13**, 10191–10200.
76 Y. Tu, F. Peng, P. B. White and D. A. Wilson, *Angew. Chem., Int. Ed.*, 2017, **56**, 7620–7624.
77 Y. Tu, F. Peng, X. Sui, Y. Men, P. B. White, J. C. M. van Hest and D. A. Wilson, *Nat. Chem.*, 2017, **9**, 480–486.
78 Y. Tu, F. Peng, J. M. Heuvelmans, S. Liu, R. J. M. Nolte and D. A. Wilson, *Angew. Chem., Int. Ed.*, 2019, **58**, 8687–8691.
79 L. K. E. A. Abdelmohsen, M. Nijemeisland, G. M. Pawar, G.-J. A. Janssen, R. J. M. Nolte, J. C. M. van Hest and D. A. Wilson, *ACS Nano*, 2016, **10**, 2652–2660.
80 H. Li, F. Peng, X. Yan, C. Mao, X. Ma, D. A. Wilson, Q. He and Y. Tu, *Acta Pharm. Sin. B*, 2023, **13**, 517–541.
81 J. Ye, Y. Fan, G. Niu, B. Zhou, Y. Kang and X. Ji, *Nano Today*, 2024, **55**, 102212.
82 X. Arqué, T. Patiño and S. Sánchez, *Chem. Sci.*, 2022, **13**, 9128–9146.
83 J. Yong, A. S. Mellick, J. Whitelock, J. Wang and K. Liang, *Adv. Mater.*, 2023, **35**, 2205746.
84 W. Gao, B. E.-F. de Ávila, L. Zhang and J. Wang, *Adv. Drug Delivery Rev.*, 2018, **125**, 94–101.
85 M. Wan, T. Li, H. Chen, C. Mao and J. Shen, *Angew. Chem., Int. Ed.*, 2021, **60**, 13158–13176.
86 C. Gao, Y. Wang, Z. Ye, Z. Lin, X. Ma and Q. He, *Adv. Mater.*, 2021, **33**, 2000512.
87 W. Liu, Y. Liu, H. Li, H. Nie, M. Tian and W. Long, *Adv. Funct. Mater.*, 2023, **33**, 2212452.
88 M. Xuan, J. Shao, X. Lin, L. Dai and Q. He, *ChemPhysChem*, 2014, **15**, 2255–2260.
89 Y. Wu, T. Si, C. Gao, M. Yang and Q. He, *J. Am. Chem. Soc.*, 2018, **140**, 11902–11905.
90 K. T. Kim, J. Zhu, S. A. Meeuwissen, J. J. L. M. Cornelissen, D. J. Pochan, R. J. M. Nolte and J. C. M. van Hest, *J. Am. Chem. Soc.*, 2010, **132**, 12522–12524.
91 D. A. Wilson, R. J. M. Nolte and J. C. M. van Hest, *J. Am. Chem. Soc.*, 2012, **134**, 9894–9897.
92 D. A. Wilson, R. J. M. Nolte and J. C. M. van Hest, *Nat. Chem.*, 2012, **4**, 268–274.
93 R. Salva, J.-F. Le Meins, O. Sandre, A. Brûlet, M. Schmutz, P. Guenoun and S. Lecommandoux, *ACS Nano*, 2013, **7**, 9298–9311.
94 L. K. E. A. Abdelmohsen, D. S. Williams, J. Pille, S. G. Ozel, R. S. M. Rikken, D. A. Wilson and J. C. M. van Hest, *J. Am. Chem. Soc.*, 2016, **138**, 9353–9356.
95 J. Xiao and J. Du, *J. Am. Chem. Soc.*, 2020, **142**, 6569–6577.

96 Q. Yan and Y. Zhao, *J. Am. Chem. Soc.*, 2013, **135**, 16300–16303.
97 J. Zhu, Z. Gong, C. Yang and Q. Yan, *J. Am. Chem. Soc.*, 2021, **143**, 20183–20191.
98 Q. Yan and Y. Zhao, *Angew. Chem., Int. Ed.*, 2013, **52**, 9948–9951.
99 N. J. Warren and S. P. Armes, *J. Am. Chem. Soc.*, 2014, **136**, 10174–10185.
100 V. Balasubramanian, B. Herranz-Blanco, P. V. Almeida, J. Hirvonen and H. A. Santos, *Prog. Polym. Sci.*, 2016, **60**, 51–85.
101 A. Blanazs, S. P. Armes and A. J. Ryan, *Macromol. Rapid Commun.*, 2009, **30**, 267–277.
102 S. Cao, J. Shao, Y. Xia, H. Che, Z. Zhong, F. Meng, J. C. M. van Hest, L. K. E. A. Abdelmohsen and D. S. Williams, *Small*, 2019, **15**, 1901849.
103 S. Cao, L. K. E. A. Abdelmohsen, J. Shao, J. van den Dikkenberg, E. Mastrobattista, D. S. Williams and J. C. M. van Hest, *ACS Macro Lett.*, 2018, **7**, 1394–1399.
104 M. Huo, Q. Ye, H. Che, X. Wang, Y. Wei and J. Yuan, *Macromolecules*, 2017, **50**, 1126–1133.
105 L. P. D. Ratcliffe, M. J. Derry, A. Ianiro, R. Tuinier and S. P. Armes, *Angew. Chem., Int. Ed.*, 2019, **58**, 18964–18970.
106 S. Varlas, T. J. Neal and S. P. Armes, *Chem. Sci.*, 2022, **13**, 7295–7303.
107 H. Liu, R. Wang, J. Wei, C. Cheng, Y. Zheng, Y. Pan, X. He, M. Ding, H. Tan and Q. Fu, *J. Am. Chem. Soc.*, 2018, **140**, 6604–6610.
108 Y. Zheng, Z. Wang, Z. Li, H. Liu, J. Wei, C. Peng, Y. Zhou, J. Li, Q. Fu, H. Tan and M. Ding, *Angew. Chem., Int. Ed.*, 2021, **60**, 22529–22536.
109 Z. Deng, S. Yuan, R. X. Xu, H. Liang and S. Liu, *Angew. Chem., Int. Ed.*, 2018, **57**, 8896–8900.
110 Q. Yan and W. Sang, *Chem. Sci.*, 2016, **7**, 2100–2105.
111 Q. Yan, R. Zhou, C. Fu, H. Zhang, Y. Yin and J. Yuan, *Angew. Chem., Int. Ed.*, 2011, **50**, 4923–4927.
112 Z. Deng, Y. Qian, Y. Yu, G. Liu, J. Hu, G. Zhang and S. Liu, *J. Am. Chem. Soc.*, 2016, **138**, 10452–10466.
113 J. Gaitzsch, X. Huang and B. Voit, *Chem. Rev.*, 2016, **116**, 1053–1093.
114 O. Rifaie-Graham, S. Ulrich, N. F. B. Galensowske, S. Balog, M. Chami, D. Rentsch, J. R. Hemmer, J. Read de Alaniz, L. F. Boesel and N. Bruns, *J. Am. Chem. Soc.*, 2018, **140**, 8027–8036.
115 R. Deng, M. J. Derry, C. J. Mable, Y. Ning and S. P. Armes, *J. Am. Chem. Soc.*, 2017, **139**, 7616–7623.
116 X. Li, Y. Wang and Q. Yan, *Angew. Chem., Int. Ed.*, 2023, **62**, e202305290.
117 M. C. M. van Oers, F. P. J. T. Rutjes and J. C. M. van Hest, *J. Am. Chem. Soc.*, 2013, **135**, 16308–16311.
118 C. K. Wong, A. F. Mason, M. H. Stenzel and P. Thordarson, *Nat. Commun.*, 2017, **8**, 1240.
119 S. Varlas, R. Keogh, Y. Xie, S. L. Horswell, J. C. Foster and R. K. O'Reilly, *J. Am. Chem. Soc.*, 2019, **141**, 20234–20248.
120 Y. Men, W. Li, G.-J. Janssen, R. S. M. Rikken and D. A. Wilson, *Nano Lett.*, 2018, **18**, 2081–2085.
121 J. Sun, S. Kleuskens, J. Luan, D. Wang, S. Zhang, W. Li, G. Uysal and D. A. Wilson, *Nat. Commun.*, 2023, **14**, 3612.
122 J. Sun, S. J. Rijpkema, J. Luan, S. Zhang and D. A. Wilson, *Nat. Commun.*, 2021, **12**, 2235.
123 Y. Men, W. Li, Y. Tu, F. Peng, G.-J. A. Janssen, R. J. M. Nolte and D. A. Wilson, *ACS Nano*, 2019, **13**, 12767–12773.
124 I. A. B. Pijpers, L. K. E. A. Abdelmohsen, D. S. Williams and J. C. M. van Hest, *ACS Macro Lett.*, 2017, **6**, 1217–1222.
125 Y. Tu, F. Peng, A. A. M. André, Y. Men, M. Srinivas and D. A. Wilson, *ACS Nano*, 2017, **11**, 1957–1963.
126 B. J. Toebes, L. K. E. A. Abdelmohsen and D. A. Wilson, *Polym. Chem.*, 2018, **9**, 3190–3194.
127 B. J. Toebes, F. Cao and D. A. Wilson, *Nat. Commun.*, 2019, **10**, 5308.
128 A. Joseph, C. Contini, D. Cecchin, S. Nyberg, L. Ruiz-Perez, J. Gaitzsch, G. Fullstone, X. Tian, J. Azizi, J. Preston, G. Volpe and G. Battaglia, *Sci. Adv.*, 2017, **3**, e1700362.
129 M. Xuan, J. Shao, X. Lin, L. Dai and Q. He, *Colloids Surf., A*, 2015, **482**, 92–97.
130 J. Feng, X. Li, T. Xu, X. Zhang and X. Du, *Acta Biomater.*, 2024, **173**, 1–35.
131 X. Ma, K. Hahn and S. Sanchez, *J. Am. Chem. Soc.*, 2015, **137**, 4976–4979.
132 Z. Ye, Y. Wang, S. Liu, D. Xu, W. Wang and X. Ma, *J. Am. Chem. Soc.*, 2021, **143**, 15063–15072.
133 X. Ma, A. C. Hortelao, A. Miguel-López and S. Sánchez, *J. Am. Chem. Soc.*, 2016, **138**, 13782–13785.
134 F. Mou, C. Chen, H. Ma, Y. Yin, Q. Wu and J. Guan, *Angew. Chem., Int. Ed.*, 2013, **52**, 7208–7212.
135 T. Maric, A. Løvind, Z. Zhang, J. Geng and A. Boisen, *Adv. Healthcare Mater.*, 2023, **12**, 2203018.
136 Y. Feng, M. An, Y. Liu, M. T. Sarwar and H. Yang, *Adv. Funct. Mater.*, 2023, **33**, 2209883.
137 B. Kherzi and M. Pumera, *Nanoscale*, 2016, **8**, 17415–17421.
138 Y. Liu, Y. Cheng, C. Zhao, H. Wang and Y. Zhao, *Adv. Sci.*, 2022, **9**, 2104272.
139 J. Parmar, D. Vilela, K. Villa, J. Wang and S. Sánchez, *J. Am. Chem. Soc.*, 2018, **140**, 9317–9331.
140 M. T. De Martino, F. Tonin, N. A. Yewdall, M. Abdelghani, D. S. Williams, U. Hanefeld, F. P. J. T. Rutjes, L. K. E. A. Abdelmohsen and J. C. M. van Hest, *Chem. Sci.*, 2020, **11**, 2765–2769.
141 I. A. B. Pijpers, S. Cao, A. Llopis-Lorente, J. Zhu, S. Song, R. R. M. Joosten, F. Meng, H. Friedrich, D. S. Williams, S. Sánchez, J. C. M. van Hest and L. K. E. A. Abdelmohsen, *Nano Lett.*, 2020, **20**, 4472–4480.
142 W. Liu, X. Chen, X. Lu, J. Wang, Y. Zhang and Z. Gu, *Adv. Funct. Mater.*, 2020, **30**, 2003195.
143 J. Zhu, T. Xiao, J. Zhang, H. Che, Y. Shi, X. Shi and J. C. M. van Hest, *ACS Nano*, 2020, **14**, 11225–11237.
144 J. Zhao, L. Wang, L. Jia, Y. Liu, S. Cao, J. Wen, W. Li and K. Yang, *Small*, 2025, **21**, 2408959.
145 J. Wang, H. Wu, X. Zhu, R. Zwolsman, S. R. J. Hofstraat, Y. Li, Y. Luo, R. R. M. Joosten, H. Friedrich, S. Cao, L. K. E. A. Abdelmohsen, J. Shao and J. C. M. van Hest, *Nat. Commun.*, 2024, **15**, 4878.

146 S. Cao, H. Wu, I. A. B. Pijpers, J. Shao, L. K. E. A. Abdelmohsen, D. S. Williams and J. C. M. van Hest, *ACS Nano*, 2021, **15**, 18270–18278.
147 Y. Hong, J. W. Y. Lam and B. Z. Tang, *Chem. Soc. Rev.*, 2011, **40**, 5361–5388.
148 A. Qin, J. W. Y. Lam and B. Z. Tang, *Prog. Polym. Sci.*, 2012, **37**, 182–209.
149 Y. Liu, X. Chen, X. Liu, W. Guan and C. Lu, *Chem. Soc. Rev.*, 2023, **52**, 1456–1490.
150 H. Chen, Y. Fan, N. Zhang, S. Trépout, B. Ptissam, A. Brûlet, B. Z. Tang and M.-H. Li, *Chem. Sci.*, 2021, **12**, 5495–5504.
151 R. Hu, A. J. Qin and B. Z. Tang, *Prog. Polym. Sci.*, 2020, **100**, 101176.
152 N. Zhang, S. Trépout, H. Chen and M.-H. Li, *J. Am. Chem. Soc.*, 2023, **145**, 288–299.
153 F. Peng, Y. Tu, Y. Men, J. C. M. van Hest and D. A. Wilson, *Adv. Mater.*, 2017, **29**, 1604996.
154 H. Che, J. Zhu, S. Song, A. F. Mason, S. Cao, I. A. B. Pijpers, L. K. E. A. Abdelmohsen and J. C. M. van Hest, *Angew. Chem., Int. Ed.*, 2019, **58**, 13113–13118.
155 Y. Tu, F. Peng and D. A. Wilson, *Adv. Mater.*, 2017, **29**, 1701970.
156 E. Karshalev, B. Esteban-Fernández de Ávila and J. Wang, *J. Am. Chem. Soc.*, 2018, **140**, 3810–3820.
157 Y. Hu, W. Liu and Y. Sun, *Adv. Funct. Mater.*, 2022, **32**, 2109181.
158 T. Liu, L. Xie, C.-A. H. Price, J. Liu, Q. He and B. Kong, *Chem. Soc. Rev.*, 2022, **51**, 10083–10119.
159 C. Chen, S. Tang, H. Teymourian, E. Karshalev, F. Zhang, J. Li, F. Mou, Y. Liang, J. Guan and J. Wang, *Angew. Chem., Int. Ed.*, 2018, **57**, 8110–8114.
160 I. Santiago, *Nano Today*, 2018, **19**, 11–15.
161 C. Chen, E. Karshalev, J. Li, F. Soto, R. Castillo, I. Campos, F. Mou, J. Guan and J. Wang, *ACS Nano*, 2016, **10**, 10389–10396.
162 J. Shao, S. Cao, H. Che, M. T. De Martino, H. Wu, L. K. E. A. Abdelmohsen and J. C. M. van Hest, *J. Am. Chem. Soc.*, 2022, **144**, 11246–11252.
163 M. Safdar, S. U. Khan and J. Jänis, *Adv. Mater.*, 2018, **30**, 1703660.
164 M. Medina-Sánchez, L. Schwarz, A. K. Meyer, F. Hebenstreit and O. G. Schmidt, *Nano Lett.*, 2016, **16**, 555–561.
165 J. Li, I. Rozen and J. Wang, *ACS Nano*, 2016, **10**, 5619–5634.
166 B. Esteban-Fernández de Ávila, A. Martín, F. Soto, M. A. Lopez-Ramirez, S. Campuzano, G. M. Vásquez-Machado, W. Gao, L. Zhang and J. Wang, *ACS Nano*, 2015, **9**, 6756–6764.
167 B. Esteban-Fernández de Ávila, P. Angsantikul, D. E. Ramírez-Herrera, F. Soto, H. Teymourian, D. Dehaini, Y. Chen, L. Zhang and J. Wang, *Sci. Robot.*, 2018, **3**, eaat0485.
168 Z. Sun and Y. Hou, *Adv. Ther.*, 2022, **5**, 2100228.
169 J. Li, B. Esteban-Fernández de Ávila, W. Gao, L. Zhang and J. Wang, *Sci. Robot.*, 2017, **2**, eaam6431.
170 T. Li, X. Chang, Z. Wu, J. Li, G. Shao, X. Deng, J. Qiu, B. Guo, G. Zhang, Q. He, L. Li and J. Wang, *ACS Nano*, 2017, **11**, 9268–9275.
171 Z. Wu, T. Li, J. Li, W. Gao, T. Xu, C. Christianson, W. Gao, M. Galarnyk, Q. He, L. Zhang and J. Wang, *ACS Nano*, 2014, **8**, 12041–12048.
172 F. Zhang, R. Mundaca-Uribe, H. Gong, B. Esteban-Fernández de Ávila, M. Beltrán-Gastélum, E. Karshalev, A. Nourhani, Y. Tong, B. Nguyen, M. Gallot, Y. Zhang, L. Zhang and J. Wang, *Adv. Mater.*, 2019, **31**, 1901828.
173 X. Wei, M. Beltrán-Gastélum, E. Karshalev, B. Esteban-Fernández de Ávila, J. Zhou, D. Ran, P. Angsantikul, R. H. Fang, J. Wang and L. Zhang, *Nano Lett.*, 2019, **19**, 1914–1921.
174 H. Xie, M. Sun, X. Fan, Z. Lin, W. Chen, L. Wang, L. Dong and Q. He, *Sci. Robot.*, 2019, **4**, eaav8006.
175 A. C. Hortelao, C. Simó, M. Guix, S. Guallar-Garrido, E. Julián, D. Vilela, L. Rejc, P. Ramos-Cabrer, U. Cossío, V. Gómez-Vallejo, T. Patiño, J. Llop and S. Sánchez, *Sci. Robot.*, 2021, **6**, eabd2823.
176 N. Ruiz-González, D. Esporrín-Ubieto, A. C. Hortelao, J. C. Fraire, A. C. Bakenecker, M. Guri-Canals, R. Cugat, J. M. Carrillo, M. Garcia-Batlletbó, P. Laiz, T. Patiño and S. Sánchez, *Small*, 2024, **20**, 2309387.
177 M. Chen, Z. Lin, M. Xuan, X. Lin, M. Yang, L. Dai and Q. He, *Angew. Chem., Int. Ed.*, 2021, **60**, 16674–16679.
178 Z. Deng, F. Mou, S. Tang, L. Xu, M. Luo and J. Guan, *Appl. Mater. Today*, 2018, **13**, 45–53.
179 H. Liu, J. Zhang, Y. Jia, X. Liu, X. Chen, W. Zhao and C. Mao, *Chem. Eng. J.*, 2022, **442**, 135994.
180 S. Venkataraman, J. L. Hedrick, Z. Y. Ong, C. Yang, P. L. R. Ee, P. T. Hammond and Y. Y. Yang, *Adv. Drug Delivery Rev.*, 2011, **63**, 1228–1246.
181 M. J. Ernsting, M. Murakami, A. Roy and S.-D. Li, *J. Controlled Release*, 2013, **172**, 782–794.
182 H. Hadji and K. Bouchemal, *J. Controlled Release*, 2022, **342**, 93–110.
183 R. Agarwal, P. Jurney, M. Raythatha, V. Singh, S. V. Sreenivasan, L. Shi and K. Roy, *Adv. Healthcare Mater.*, 2015, **4**, 2269–2280.
184 Z. Song, J. Fang, Z. Wang, R. Xiao, X. Guo and S. Zhou, *Adv. Funct. Mater.*, 2023, **33**, 2212326.
185 S. Barua, J.-W. Yoo, P. Kolhar, A. Wakankar, Y. R. Gokarn and S. Mitragotri, *Proc. Natl. Acad. Sci. U.S.A.*, 2013, **110**, 3270–3275.
186 V. P. Chauhan, Z. Popović, O. Chen, J. Cui, D. Fukumura, M. G. Bawendi and R. K. Jain, *Angew. Chem., Int. Ed.*, 2011, **50**, 11417–11420.
187 G. Chen, I. Roy, C. Yang and P. N. Prasad, *Chem. Rev.*, 2016, **116**, 2826–2885.
188 A. M. López-Estévez, P. Lapuhs, L. Pineiro-Alonso and M. J. Alonso, *Adv. Mater.*, 2024, **36**, 2309355.
189 J. Xu, M. Song, Z. Fang, L. Zheng, X. Huang and K. Liu, *J. Controlled Release*, 2023, **353**, 699–712.
190 X. Hu, Y. Zhang, Z. Xie, X. Jing, A. Bellotti and Z. Gu, *Biomacromolecules*, 2017, **18**, 649–673.
191 M. Wei, Y. Gao, X. Li and M. J. Serpe, *Polym. Chem.*, 2017, **8**, 127–143.

192 M. Sousa de Almeida, E. Susnik, B. Drasler, P. Taladriz-Blanco, A. Petri-Fink and B. Rothen-Rutishauser, *Chem. Soc. Rev.*, 2021, **50**, 5397–5434.
193 E.-K. Lim, T. Kim, S. Paik, S. Haam, Y.-M. Huh and K. Lee, *Chem. Rev.*, 2015, **115**, 327–394.
194 J. Wang, R. Dong, H. Wu, Y. Cai and B. Ren, *Nano-Micro Lett.*, 2019, **12**, 11.
195 H. Kim, K. Jo, H. Choi and S. K. Hahn, *J. Controlled Release*, 2024, **374**, 606–626.
196 S. Cao, Y. Xia, J. Shao, B. Guo, Y. Dong, I. A. B. Pijpers, Z. Zhong, F. Meng, L. K. E. A. Abdelmohsen, D. S. Williams and J. C. M. van Hest, *Angew. Chem., Int. Ed.*, 2021, **60**, 17629–17637.
197 N. Zhang, H. Chen, Y. Fan, L. Zhou, S. Trépout, J. Guo and M.-H. Li, *ACS Nano*, 2018, **12**, 4025–4035.
198 D. Zhang, Y. Fan, H. Chen, S. Trépout and M.-H. Li, *Angew. Chem., Int. Ed.*, 2019, **58**, 10260–10265.
199 R. Hu, N. L. C. Leung and B. Z. Tang, *Chem. Soc. Rev.*, 2014, **43**, 4494–4562.
200 M. Gao and B. Z. Tang, *Coord. Chem. Rev.*, 2020, **402**, 213076.
201 S. Cao, J. Shao, H. Wu, S. Song, M. T. De Martino, I. A. B. Pijpers, H. Friedrich, L. K. E. A. Abdelmohsen, D. S. Williams and J. C. M. van Hest, *Nat. Commun.*, 2021, **12**, 2077.
202 F. Hu, S. Xu and B. Liu, *Adv. Mater.*, 2018, **30**, 1801350.